Annu. Rev. Nucl. Part. Sci. 1995. 45:337–90

THE NUCLEAR EMC EFFECT

D. F. Geesaman

Physics Division, Argonne National Laboratory, 9700 South Cass Avenue, Argonne, Illinois 60439-4843

K. Saito

Physics Division, Tohoku College of Pharmacy, Sendai 981, Japan

A. W. Thomas

Department of Physics and Mathematical Physics, University of Adelaide, SA 5005, Australia

---

CONTENTS

0163-8998/95/1201-0337$5.00

KEY WORDS: quarks, partons, structure functions, nuclei, shadowing

ABSTRACT

Deep-inelastic scattering reactions provided the first clear evidence that the quark structure of nucleons and nuclei were significantly different. We review the progress in understanding the nuclear dependence of deep-inelastic scattering reactions and parton distributions—the nuclear EMC effect. While there is now a considerable body of high-quality deep-inelastic data, more work is required to exploit other hard probes with differing sensitivities to quark-flavor and gluon degrees of freedom. A variety of models for the nuclear dependence of structure functions are also considered. Substantial progress has been made in establishing the validity of these models and it is now clear what must be included in any realistic treatment. Nevertheless, it is not yet possible to identify a definitive set of mechanisms that account satisfactorily for the experimental nuclear dependence.

1. INTRODUCTION

The distribution of quarks in a nucleus differs significantly from the distribution of quarks in the nucleon. This became clear when, more than a decade ago, the European Muon Collaboration (EMC) measured the ratios of structure functions of iron and deuterium in the deep-inelastic scattering (DIS) of muons (1). Over the past decade, nuclear and particle physicists have strived to understand this result. Their efforts have led to a far better understanding of the implications of quantum chromodynamics (QCD) in a many-body system such as the nucleus. The early optimism that a simple mechanism would be discovered that would reveal new collective features of nonperturbative QCD has given way to systematic studies over a wide range of experimental observables and a thorough theoretical examination of the properties of nuclear currents.

The ratio of structure functions of iron and copper to deuterium is presented in Figure 1. This ratio can be compared with the original EMC results shown as an inset in the figure. The data are plotted vs Bjorken x, which measures the fraction of the light-cone momentum of the nucleon carried by the struck quark in the so-called Bjorken limit (see Section 2). The data have three major features. The significant reduction in the ratio from a value of 1 for $0.3 < x < 0.6$ is generally referred to as the EMC effect. The reduction for

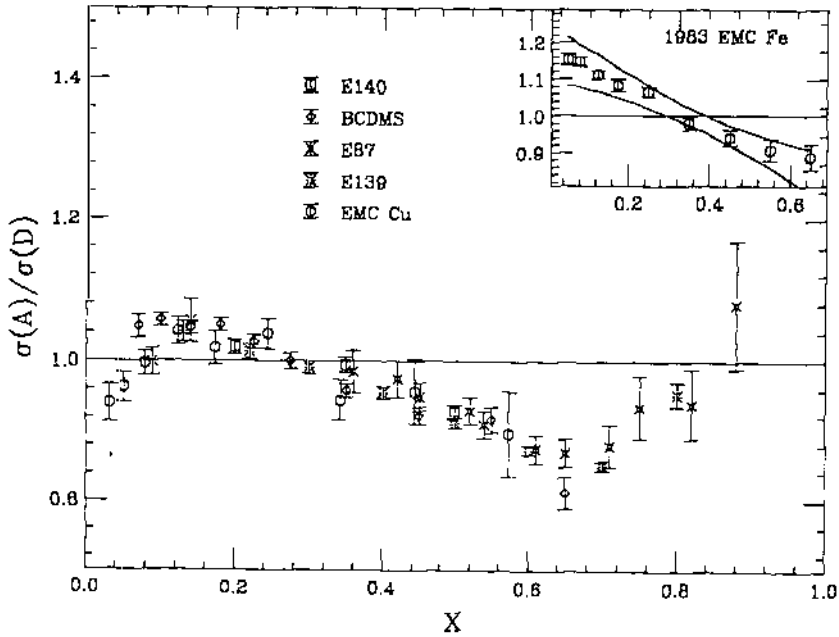

Figure 1 Ratios of the deep-inelastic cross sections on targets of iron or copper to those of deuterium (2–6). The insert contains the original EMC data, which have an additional 7% overall multiplicative uncertainty (1).

$x < 0.1$ is called shadowing and is analogous to the reduction in cross sections observed in real-photon reactions. The nucleon structure function must vanish as x approaches 1.0, so here and at $x > 1.0$ the structure function arises purely from nuclear effects, the simplest of which is the intrinsic motion of the nucleons in a nucleus at rest. Each of these regions has unique sensitivities to different many-body effects. The rise of the ratio above unity for x around 0.1–0.2 represents a transition region in the data and in the models.

In this chapter, we review the progress of the past decade in the study of quark distributions of nuclei. In Section 2, we review the parton model and the QCD results, which form the foundation of our understanding of quark distributions. The various theoretical models to explain the nuclear dependence of the quark distributions are introduced in Section 3. Section 4 contains a discussion of the features of the experimental results, and in Section 5 we outline recent theoretical progress. Finally, in Section 6 we summarize the current status of the nuclear EMC effect and present the directions we feel most urgently need to be taken or that appear most promising for future work.

2. INTRODUCTION TO DEEP-INELASTIC SCATTERING

Consider the inclusive scattering of a high-energy lepton, with initial energy (four-momentum) E (k), final energy E' (k'), and scattering angle θ, from a hadronic target of mass M and initial four-momentum p. We denote the spacelike four-momentum transferred to the target as q. For an unpolarized target, the laboratory differential cross section for electromagnetic scattering involves the lepton tensor $L_{\mu\nu}$:

$$L_{\mu\nu} = k_\mu k'_\nu + k'_\mu k_\nu + \frac{1}{2} g_{\mu\nu} q^2, \qquad 1.$$

and the hadronic tensor $W^{\mu\nu}$:

$$W^{\mu\nu} = \tilde{g}^{\mu\nu} W_1 + \frac{\tilde{p}^\mu \tilde{p}^\nu}{M^2} W_2,$$

$$\tilde{g}^{\mu\nu} = -g^{\mu\nu} + \frac{q^\mu q^\nu}{q^2},$$

$$\tilde{p}^\mu = p^\mu - \frac{p \cdot q}{q^2} q^\mu. \qquad 2.$$

After contracting the tensors and integrating over phase space, we find

$$\frac{d^2\sigma}{dE' d\Omega} = \frac{4\alpha^2 (E')^2}{q^4} \left(\frac{F_2}{\nu} \cos^2 \frac{\theta}{2} + 2 \frac{F_1}{M} \sin^2 \frac{\theta}{2} \right). \qquad 3.$$

All of the information about the structure of the target is now contained in the structure functions F_1 ($\equiv MW_1$) and F_2 ($\equiv \nu W_2$, where $\nu = E - E'$ is the photon energy in the laboratory frame), which can depend on at most two variables. These variables are usually chosen to be the Lorentz invariant quantities $Q^2 (= -q^2 > 0)$ and Bjorken x ($= -q^2/2p \cdot q = Q^2/2M\nu$). In terms of these new variables, the differential cross section takes the form:

$$\frac{d^2\sigma}{dx dQ^2} = \frac{4\pi\alpha^2 (E')^2}{xQ^4} \frac{E'}{E} \left(F_2 \cos^2 \frac{\theta}{2} + 2 \frac{\nu}{M} F_1 \sin^2 \frac{\theta}{2} \right). \qquad 4.$$

For (anti-)neutrino scattering from an unpolarized target, we find a third structure function, F_3, associated with parity violation:

$$\frac{d^2\sigma^{\nu(\bar{\nu})}}{dE' d\Omega} = \frac{G_F^2 (E')^2}{2\pi^2} \left(\frac{M_W^2}{M_W^2 + Q^2} \right)^2$$

$$\left(\frac{F_2^{\nu(\bar{\nu})}}{\nu} \cos^2 \frac{\theta}{2} + 2 \frac{F_1^{\nu(\bar{\nu})}}{M} \sin^2 \frac{\theta}{2} \pm \frac{E + E'}{M\nu} F_3^{\nu(\bar{\nu})} \sin^2 \frac{\theta}{2} \right). \qquad 5.$$

2.1 *The Parton Model*

In the late 1960s, tremendous excitement was generated by the discovery at SLAC that in the Bjorken limit (Q^2 and $\nu \to \infty$ with x fixed), the structure functions were almost independent of Q^2 over a very wide range. That is, they were functions of a single variable—Bjorken x. This result is what one would expect if the nucleon contained a collection of elementary constituents (initially called partons by Feynman but later identified with quarks) with low mass that do not interact strongly during the DIS collision.

For simplicity, we consider this problem in a so-called infinite momentum frame, e.g. one in which the nucleon has momentum $P \gg M_N$ (M_N is the nucleon mass) in the z direction so that its four-momentum is $p = (P; 0, 0, P)$. Suppose a constituent with four-momentum $yp = (yP; 0, 0, yP)$, where y is the momentum fraction of the nucleon carried by the constituent, absorbs the photon. Its final invariant mass squared will be

$$(yp + q)^2 = (yp)^2 - Q^2 + 2y\ p \cdot q. \qquad 6.$$

The invariant mass squared of the parton, $(yp)^2$ and $(yp+q)^2$, is small compared with Q^2 and $p \cdot q$. Thus we find $y = Q^2/2p \cdot q$, which was termed Bjorken x above. Therefore, under the assumptions of the parton model, only a parton with fraction x of the momentum of the nucleon can absorb the exchanged photon (or W boson). If the impulse approximation is valid, DIS structure functions can then be used to measure the number density of partons in the nucleon with momentum fraction x.

It is usual to define distributions $q(x)$ ($q = u, d, s$, etc), which give the number density of quarks in the target. For example, $u(x)xdx$ gives the fraction of momentum of u quarks in the proton with momentum between xP and $(x + dx)P$ in the infinite momentum frame. By charge symmetry, u also gives the distribution of d quarks in the neutron. The assumption of charge symmetry is so deeply ingrained that it is rarely noted as an approximation in textbooks. However, recent studies have suggested that, at least for the minority valence distribution (d^p), it may be broken to a surprisingly large extent (7, 8).

The structure functions mentioned above are directly related to these distribution functions. For an electromagnetic probe, we find

$$F_1(x) = \frac{1}{2}\sum_q e_q^2[q^\uparrow(x) + q^\downarrow(x)], \qquad 7.$$

$$F_2(x) = 2xF_1(x), \qquad 8.$$

where e_q is the charge in units of e of the quark of flavor q. Equation 8 is the Callan-Gross relation and relies on the partons having spin 1/2 and no transverse

momentum in the infinite momentum frame. (Note that the arrow indicates the helicity of the struck quark relative to that of the target proton.) In general, we have

$$F_2 = 2xF_1 \frac{1+R}{1+2M_N x/\nu}, \qquad 9.$$

where R is the ratio of cross sections for absorbing a longitudinal to that for a transverse photon. Experimentally, R is small (9) ($\lesssim 0.1$) for $x \gtrsim 0.1$ and for $Q^2 \gtrsim 5$ GeV^2 (see Section 4.3 for details of its A dependence).

For neutrino scattering from an isoscalar target, we find

$$F_2^{(\bar{\nu})} = x(u + \bar{u} + d + \bar{d} + s + \bar{s}), \qquad 10.$$

which measures the total quark content of the target. More important, by averaging ν and $\bar{\nu}$ data, one can measure the combination

$$F_3^{(\nu,\bar{\nu})} = u - \bar{u} + d - \bar{d}, \qquad 11.$$

which isolates the excess of quarks over antiquarks, i.e. the valence quark distribution of the nucleon. Clearly, we would expect the integral of F_3 to be

$$\int_0^1 dx\ F_3^{(\nu,\bar{\nu})}(x) = 3, \qquad 12.$$

the number of valence quarks. This equation is the Gross–Llewellyn Smith sum rule.

Initially, the major experimental activity in this field was at SLAC, but in the past 10–20 years, important work with muon and neutrino beams has been done at CERN and Fermilab, and new kinematic regions have recently become accessible at HERA. For a thorough summary of the experiments at these laboratories, we refer the reader to the review by Morfin (10) and to Section 4 of this article. Although most of the data correspond to values of Q^2 between 5 and 20 GeV^2 and values of x between 0.1 and 0.65, values of Q^2 as high as 200 GeV^2 and values of x as low as 10^{-4} have been obtained. Experimentally, the antiquarks, which form half of the sea of virtual q-$\bar{q}$ pairs in the nucleon, are concentrated at low x ($x \lesssim 0.3$). The valence quarks (see Equation 11) dominate the large x region. When one allows for the appropriate charges, the weak and electromagnetic experiments are in impressive agreement. Because of systematic errors, data sets on the same target may differ by as much as 10–20%. These differences are typically within the quoted systematic errors and can be important when an absolute measurement is required.

The experimental data show that even in the Bjorken scaling region, the structure functions have a weak Q^2 dependence, and therefore so do the distribution

functions, which we write as $q(x, Q^2)$. If one data set is used consistently to (partially) avoid systematic errors, this variation of the structure functions (scaling violation) is essentially logarithmic. To understand it, one must go beyond the naive parton model to QCD.

2.2 *Scaling Violations*

When developing a theoretical description of the deep-inelastic process, it is assumed that the wavefunction of the target has no high transverse-momentum components (i.e. $\mathbf{k}_T^2 \ll Q^2$). Thus any Q^2 dependence can come only from the lepton-quark scattering process. Once the trivial Q^2 dependence of the Mott cross section is factored out, scaling results if the quark is treated as pointlike. On the other hand, in an interacting field theory, the lepton-quark scattering amplitude involves color radiative corrections, some of which add coherently (e.g. wavefunction and vertex renormalization) and some of which are incoherent (e.g. bremsstrahlung). Such radiative processes lead to corrections that vary logarithmically with the appropriate cut-off scale, in this case Q^2.

For explicit calculations of these radiative corrections, we refer the reader to some excellent texts (11–18). It is important to develop a physical interpretation of this Q^2 variation so that it can be applied to other systems. The physics behind the Q^2 variation is perhaps best expressed through Close's "onion skin" picture, whereby every time Q^2 is increased, the resolution at which we observe the structure of the target is increased as well, revealing more and more of its previously virtual quarks and gluons. The mathematical description of the variation of the structure function with Q^2 is given by the Altarelli-Parisi equations. If one of the data sets mentioned above is used consistently (in order to avoid systematic errors), the Q^2 variation of the structure functions is well described by these equations. However, discrepancies exist between data sets, and a consistent fit to the EMC data on different nuclear targets has been difficult to achieve.

The most rigorous approach to the calculation of structure functions and to the description of their Q^2 variation comes through the operator product expansion (OPE) and the renormalization group. As these have been discussed in many texts, we highlight only those features germane to our discussion, namely the prediction of structure functions from particular quark models.

2.3 *Operator Product Expansion*

Because electromagnetic DIS involves a total cross section for lepton scattering with a single photon exchange, the structure functions are proportional (through the optical theorem) to the imaginary part of the forward Compton amplitude

for a photon of four-momentum q. The Compton amplitude is written

$$T_{\mu\nu} = i \int d^4z\, e^{iq\cdot z} \langle N|T[j_\mu(z) j_\nu(0)]\,|N\rangle, \qquad 13.$$

where j_μ is the electromagnetic current operator. The essential idea of the OPE is that the time-ordered product of the currents can be expanded in what is essentially a generalization of the familiar Taylor series. That is, one writes an infinite series whose terms each include a (possibly singular) function of z^2 times a local operator formed from $\bar{\psi}(0)$ and derivatives of $\psi(0)$ contracted with products of z^λ. This expansion of the operator is target independent.

Omitting the Lorentz indices on the current for purposes of illustration gives schematically

$$T[j(z)j(0)] = \sum_{i,n} \tilde{C}_{i,n}(z^2)\, z_{\mu_1} \cdots z_{\mu_n}\, O_{i,n}^{\mu_1 \cdots \mu_n}, \qquad 14.$$

where, for example, one might have an operator $O_{i,n}^{\mu_1 \cdots \mu_n}$ of spin n of the form:

$$\bar{\psi}(0)\gamma^{\mu_1} D^{\mu_2} \cdots D^{\mu_n} \psi(0), \qquad 15.$$

$$\bar{\psi}(0)\gamma^{\mu_1} D^{\mu_2} \psi(0) \bar{\psi}(0)\gamma^{\mu_3} \cdots D^{\mu_n} \psi(0), \qquad 16.$$

and so on. [D^μ, which has mass dimension 1, is the gauge-covariant derivative for QCD defined by $\nabla^\mu + ig\boldsymbol{\lambda}/2 \cdot \mathbf{A}^\mu$, where $\mathbf{A}^\mu$ is the vector potential for the gluon field, g is the strong coupling constant, and $\boldsymbol{\lambda}$ is a generator of color $SU(3)$.] Now, ignoring renormalization, ψ has dimensions of (energy)$^{3/2}$, which is usually called simply dimension 3/2. Therefore, the left-hand side of Equation 14 has dimension 6. If the operator $O_{i,n}$ has dimension N_i, then $\tilde{C}_{i,n}$ must have dimension $6 + n - N_i$. After Fourier transformation to give the Compton amplitude (Equation 13), the amplitude will behave like Q^{6+n-N_i}. Since $Q^2 \to \infty$ in the Bjorken limit, the dominant operators will be those with the largest exponent or the smallest value of $N_i - n$ (usually called twist). The operator in Equation 15 is twist-2, while that in Equation 16 is twist-4. In the Bjorken limit, DIS will be entirely determined by the operators of lowest twist, twist-2.

The operator given in Equation 15 is called a singlet, twist-2 operator because it involves a trace over flavors. The only other twist-2, singlet operator involves the gluons:

$$g_{\alpha\beta} F^{\mu_1\alpha} D^{\mu_2} \cdots D^{\mu_{n-1}} F^{\mu_n\beta}. \qquad 17.$$

The corresponding color stress tensor, $F^{\mu\nu a}$, in Equation 17 is $\nabla^\mu A^{\nu a} - \nabla^\nu A^{\mu a} + g f^{abc} A^{\nu b} A^{\nu c}$, where a, b, and c are color indices. One can also write down a set of nonsinglet operators

$$\bar{\psi}(0)\gamma^{\mu_1} D^{\mu_2} \cdots D^{\mu_n} \lambda_i \psi(0), \qquad 18.$$

where λ_i are now the flavor-$SU(3)$ matrices. For simplicity, we concentrate on the nonsinglet operators here.

In general, the matrix elements of these operators must be of the form

$$\left\langle N\left|O_i^{\mu_1\cdots\mu_n}\right|N\right\rangle = p^{\mu_1}\cdots p^{\mu_n}\,\langle N|O_{i,n}|N\rangle. \qquad 19.$$

Returning to Equation 13, we realize that the Fourier transform of z_μ is essentially q_μ/Q^2, which contracted with p^μ gives $1/x$. Thus we find that in the large Q^2 limit, schematically (i.e. corresponding to Equation 14)

$$T \sim \sum_n C_n(Q^2)\, x^{-n}\,\langle N|O_n|N\rangle. \qquad 20.$$

We have incorporated an appropriate number of factors of Q^{-2} into the (nth derivative of) Fourier transform of $\tilde{C}_n$ to make C_n dimensionless.

2.4 *The Renormalization Group*

The arguments just presented must be modified in a field theory like QCD. The matrix element of the currents on the left-hand side of Equation 14 and the matrix elements of the operators in the OPE on the right-hand side of the equation must be renormalized. This procedure introduces a new mass scale (or renormalization scale) μ^2, on which no physical results can depend. The μ^2 dependence of the coefficient functions $C_{i,n}[Q^2, \mu^2, g^2(\mu^2)]$ must be chosen such that Equation 13 is true after renormalization. From a practical point of view, the operator relationship must hold independent of the target. One can therefore calculate the μ^2 dependence for a simple target, such as a free quark. As this dependence is covered in many texts (11–16), we give only a brief review here.

Assuming that the operator O_n is multiplicatively renormalized by $Z_{O_n}^{-1}$, we define

$$\beta(g) = \frac{\partial g(\mu^2)}{\partial \ln \mu^2} \qquad 21.$$

and

$$\gamma_{O_n} = \frac{\partial \ln Z_{O_n}}{\partial \ln \mu^2}. \qquad 22.$$

(Note that we have dropped the label i for convenience.) Since the product $C_n\langle N|O_n|N\rangle$ is measurable, it cannot depend on μ^2. (It is proportional to the nth moment of the DIS structure function defined in Equation 31 below.) Thus we may write

$$\mu\frac{d}{d\mu}C_n\langle N|O_n|N\rangle = 0, \qquad 23.$$

and (in an appropriate gauge) after some standard calculation, we obtain

$$C_n[Q^2, \mu^2, g^2(\mu^2)] = C_n[Q^2, Q^2, g^2(Q^2)] \exp\left[-\int_{g(\mu^2)}^{g(Q^2)} \frac{\gamma}{\beta} \right] \qquad 24.$$

In practice, a series expansion for $\gamma(g')$ and $\beta(g')$ is carried to only a few terms. In leading order, we have

$$\beta(g) = -\frac{\beta}{16\pi^2}, \gamma(g) = \gamma_0^n \frac{g^2}{16\pi^2}, \qquad 25.$$

and

$$C_n[Q^2, Q^2, g^2(Q^2)] = 1. \qquad 26.$$

The integral in Equation 24 is then easily performed, and we find

$$C_n(Q^2, \mu^2, g^2) \overset{L.O.}{=} \left[\frac{\alpha_s(Q^2)}{\alpha_s(\mu^2)} \right]^{d_0^n}. \qquad 27.$$

Using the calculated value of β_0 (for N_f quark flavors) and γ_0^n, the anomalous dimension d_0^n is

$$d_0^n = \frac{\gamma_0^n}{2\beta_0} = \frac{4}{33 - 2N_f} \left[1 - \frac{2}{n(n+1)} + 4 \sum_{m=2}^{n} m^{-1} \right]. \qquad 28.$$

2.5 *The Moments of the Structure Functions*

There is a direct connection between the moments of the measured structure functions and the Compton amplitude that we have calculated to date. In fact, as a function of ν for fixed Q^2, $T_{\mu\nu}$ has two cuts: (ν_{th}, ∞), which corresponds to the physical region, and $(-\infty, -\nu_{th})$, which corresponds to crossed processes. In terms of x, again for fixed Q^2, the corresponding cuts run from (0, 1) and (−1, 0). Thus the dispersion relation for $T_{\mu\nu}$ at fixed Q^2 has the form

$$T_{\mu\nu}(x, Q^2) \frac{1}{2\pi i} \left(\int_{-\infty}^{-\nu_{th}} + \int_{\nu_{th}}^{\infty} \right) \frac{d\nu' \mathrm{disc} T_{\mu\nu}(x', Q^2)}{\nu' - \nu}. \qquad 29.$$

[Here, disc$T$ is the discontinuity of the Compton amplitude across the real axis.] Changing the integration variable from ν' to x' and using the optical theorem to replace $\mathrm{Im}T_{\mu\nu}$ with the total cross section, which is by definition the structure function, we find

$$T_{\mu\nu}(x, Q^2) = \sum_n x^{-n} \int_0^1 dx' (x')^{n-1} W_{\mu\nu}(x', Q^2). \qquad 30.$$

Note that for the various terms in $T_{\mu\nu}$, the sum over n is restricted to even or odd values, depending on the crossing properties of the corresponding piece of $W_{\mu\nu}$.

Comparing Equation 30 with Equation 20, we see that the product of the coefficient function C_n and the operator matrix element is measurable. Indeed, it is equal to the moment of the appropriate structure function, defined as

$$M_n = \int_0^1 dx x^{n-2} F(x), \qquad 31.$$

where F is F_2, xF_3, etc. The result of the above analysis based on the OPE and the renormalization group shows that the Q^2 variation of the moments of the structure functions is given by perturbative QCD. To leading order, we find

$$M_n(Q^2) = M_n(Q_0^2)\left[\frac{\alpha(Q^2)}{\alpha(Q_0^2)}\right]^{d_0^n}. \qquad 32.$$

Then for fixed Q_0^2,

$$\ln M_n(Q^2) = \frac{d_0^n}{d_0^m} \ln M_m(Q^2) + \text{constant}, \qquad 33.$$

and therefore a log-log plot of any two moments should be a straight line whose slope is predicted by QCD.

Given an analytic continuation of a set of moments $M_n(Q^2)$, the corresponding structure function can be reconstructed using a standard method known as the inverse Mellin transform (IMT):

$$xF_3(x, Q^2) = \frac{1}{2\pi i}\int_{K-i\infty}^{K+i\infty} dn\, x^{1-n} M_{3,n}(Q^2). \qquad 34.$$

(Here, K is chosen so that the integral exists.) If the moments can be written as a product, as in Equation 20, then

$$M_{3,n}(Q^2) = C_n(Q^2, \mu^2)\langle N|O_n(\mu^2)|N\rangle, \qquad 35.$$

where xF_3 is just a convolution of the IMT of C_n (denoted by $\mathcal{C}_3$) and $\langle N|O_n|N\rangle$ (denoted $\mathcal{F}_3$), i.e.

$$xF_3(x, Q^2) = \int_x^1 \frac{dy}{y} \mathcal{C}_3(x/y, Q^2, \mu^2)\left[y\mathcal{F}_3(y, \mu^2)\right]. \qquad 36.$$

This result is extremely important. In particular, $\mathcal{C}_3$ is totally independent of the structure of the target—a property known as factorization. Clearly, if we can evaluate the structure function of the target at any renormalization scale μ^2, Equation 36 allows us to calculate it at all higher values of Q^2. Higher-order

QCD corrections do not alter this result in principle; they just make C_3 more difficult to compute. For this reason, μ^2 cannot be too low.

The above discussion of Q^2 evolution involves only nonsinglet operators. The Q^2 evolution of the operators given in Equations 15 and 17 is more complicated because these operators mix under renormalization. Although the corresponding analysis is not much more difficult (it involves a 2×2 matrix), to explain it here would be too great a diversion from our main focus. Instead, we refer the reader to the appropriate texts (11–18). For example, Altarelli (17) gives a concise summary in Table 2 of his review.

2.6 *The Connection to Familiar Quark Models*

At last we have collected all the results necessary to understand how to relate quark models to QCD. Of course, if one could use nonperturbative QCD (e.g. on the lattice) to calculate $\langle N|O_n(\mu^2)|N\rangle$, these models would be unnecessary. However, such calculation is not feasible for more than a few moments at present [see for example Lissia et al (19) and Martinelli & Sachrajda (20)]. Since the models are only "QCD motivated," the connection cannot be rigorous, but we know of no sensible alternative.

Apart from lattice technology, the only known technique for solving a bound-state problem in field theory is to make quantum corrections about a classical solution. We assume that whatever quark model we are using represents just such a solution, renormalized at some scale μ^2. Although physically measurable quantities cannot depend on μ^2, the classical approximation may be better for some value. We treat the value of μ^2 appropriate to a given model, which we shall call Q_0^2, as a free parameter. If one can evaluate the twist-2 target matrix elements within the model, then using Equations 35 and 36, one can calculate the twist-2 structure function at all Q^2. Even though the twist-2 contribution may not be dominant at Q_0^2, the general considerations presented earlier (see the discussion of higher twist following Equation 16) ensure that at high enough Q^2, it will eventually dominate.

The most convenient practical method for evaluating the twist-2 moments of the structure function of a particular target comes from important work by Jaffe (21). In the $A^+ = 0$ gauge, we find that the quark and antiquark distributions at a scale Q_0^2 (characteristic of the model) are, respectively (22, 23):

$$q(x, Q_0^2) = \frac{M}{2\pi} \int_{-\infty}^{\infty} dz e^{-iMxz} \langle N|\psi_+^\dagger(\xi^-)\psi_+(0)|N\rangle_c \qquad 37.$$

and

$$\bar{q}(x, Q_0^2) = \frac{M}{2\pi} \int_{-\infty}^{\infty} dz e^{-iMxz} \langle N|\psi_+(\xi^-)\psi_+^\dagger(0)|N\rangle_c. \qquad 38.$$

Here M is the mass at the target state $|N\rangle$, c denotes a connected matrix element, and $\psi_+(\xi^{--})$ is an abbreviated notation for $1/2(1 + \alpha^3)\psi(z; 0, 0, -z)$. These equations have been applied to the MIT bag model with considerable phenomenological success (24).

3. INITIAL THEORETICAL CONSIDERATIONS

The initial shock generated by the EMC effect (1; Figure 1) led to an enormous amount of theoretical work on both the nucleon and nuclear structure functions. Since the technique of perturbative QCD can be used to describe the evolution of nuclear structure functions as well as nucleon structure functions, the origin of the EMC effect may be attributed to nonperturbative effects, about which we know very little. At present, we can only discuss nonperturbative effects in terms of models. This section is devoted to some interpretations of the EMC effect that have guided the thinking in the field. This subject is the focus of a number of other reviews as well [see e.g. Pirner (25), Barone & Predazzi (26), Berger & Coester (27), Frankfurt & Strikman (28), Rith (29), Bickerstaff & Thomas (30), Roberts (31), Barone et al (32), and Arneodo (33)].

3.1 *Multiquark Clusters*

In quark cluster models, it is assumed that a nucleus is partly made up of multinucleon clusters containing $3N$ quarks ($N = 2, 3, 4, \ldots$). As early as 1976, Krzywicki (34) had predicted a difference between the nucleon and the nuclear structure functions, in keeping with this assumption.

According to the quark-counting rule (35), the behavior of the quark momentum distributions for large x ($\sim M_c/M_N$, M_c is the mass of the target cluster) is related to the number of spectator quarks in the target. If a nucleus consists of noninteracting nucleons and multiquark clusters with some probabilities, then the valence quark distribution in a nucleus is softened in the intermediate x region. Neglecting Fermi motion, the structure function of the nucleon ($3q$ state) vanishes for $x \geq 1$, while that of the multiquark state extends beyond $x = 1$. Since both structure functions are normalized, the momentum carried by the valence quark in the cluster is smaller than that in the nucleon for $0 < x < 1$.

In the early and mid-1980s, many authors pursued this idea with clusters of 6, 9, 12... quarks to fit the original EMC data [see e.g. Pirner & Vary (36), Carlson & Havens (37), Daté & Nakamura (38), Daté (39), Faissner & Kim (40), Daté et al (41), Vary (42), Faissner et al (43), Chemtob & Peshanski (44), Dias de Deus et al (45), Clark et al (46), Kondratyuk & Shmatikov (47), Vary & Harindranath (48), Kisslinger & Johnson (49), Lassila & Sukhatme (50), and Barshay & Rein (51)].

Whether such multiquark clusters occur in a nucleus is a very basic but exciting question in nuclear physics (52). However, at the present experimental stage, we have little real understanding of nuclear structure functions for large x ($\gtrsim M_c/M_N$), where the multiquark states would be expected to contribute (see Section 4.8).

3.2 *Dynamical Rescaling*

Nachtmann et al (53) and Close et al (54) independently noted that the differences between nuclear structure functions might result from a difference in the scale of confinement of the nuclear constituents. Indeed, these authors discovered that the structure functions of iron and deuterium could be related to each other in the middle x region by a relative shift in the scale of the measurements ($Q^2 \to \xi_A Q^2$).

To see how this relation works, we consider the moments of the nuclear structure function $F_2^A(x, Q^2)$, defined by (see Equation 31)

$$M_n^A(Q^2) = \int_0^A dx x^{n-2} F_2^A(x, Q^2). \qquad 39.$$

If one knows $M_n^A(Q^2)$ at some initial value of low Q^2, say μ_A^2, then it is calculable for all $Q^2 > \mu_A^2$ with perturbative QCD (see Equation 32). The idea of dynamical rescaling is that, since in perturbative QCD the target dependence resides in the nonperturbative matrix elements, the scale μ_A^2 may be target dependent and independent of n, such that

$$M_n^A(\mu_A^2) = M_n^N(\mu_N^2). \qquad 40.$$

Then, we find for $Q^2 > \mu_A^2$

$$M_n^A(Q^2) = M_n^N(\xi_A Q^2), \qquad 41.$$

with

$$\xi_A = \left(\frac{\mu_A^2}{\mu_N^2}\right)^{-\frac{\alpha_s(\mu_A^2)}{\alpha_s(Q^2)}} \qquad 42.$$

The IMT (defined by Equation 34) of Equation 41 gives the relation between the nucleon and nuclear structure functions as

$$F_2^A(x, Q^2) = F_2^N(x, \xi_A Q^2). \qquad 43.$$

Let r_N (r_A) be the size of the free (bound) nucleon. If one supposes that

$$\mu_{N(A)} \propto \frac{1}{r_{N(A)}}, \qquad 44.$$

ξ_A can be related to the confinement sizes of the free and bound nucleons as

$$\xi_A = \left(\frac{r_N^2}{r_A^2}\right)^{-\frac{\alpha_s\left(\mu_N^2 r_N^2/r_A^2\right)}{2}}. \qquad 45.$$

Nachtmann & Pirner (53) and Close et al (54, 55) [see also Gupta et al (56)] proposed that quarks in heavier nuclei are confined in a region larger in size than in the free nucleon. Close et al suggested that the ratio r_A/r_N would be provided by interpolation between the confinement size of the isolated nucleon and that of two totally overlapping nucleons as

$$\left(\frac{r_A}{r_N}\right) = 1 + V_A\left(\frac{r_{tot}}{r_N} - 1\right), \qquad 46.$$

where V_A is the fraction of the volume of the nucleon that overlaps another nucleon and $r_{tot} = 2^{1/3} r_N$, e.g. $r_{He}/r_N \simeq 1.04$; $r_{Fe}/r_N \simeq 1.15$; and $r_{Pb}/r_N \simeq 1.19$. As A becomes large, V_A increases gradually. This idea is developed further in References 57–59. Nachtmann et al speculated that the confinement size depends on resolution so that for large enough Q^2, quarks become completely deconfined in a nucleus, i.e. r_A becomes the nuclear radius (60, 61).

The question raised by these models is how the successful, traditional picture of a nucleus as a collection of bound nucleons can be reconciled with this simple idea, which seems to present a completely different picture of atomic nuclei (62). Some of the theoretical assumptions in the dynamical rescaling model still seem to be on soft ground [see also Cleymans & Thews (63)]. Using the inclusive electron-nucleus scattering data analyzed as quasifree electron-nucleon scattering, Sick (64) pointed out that the increase in size of a bound nucleon in a nucleus is quite small, e.g. $r_{Fe}/r_N < 1.06$ [see also Mulders (65)].

3.3 *Nuclear Binding in the Convolution Formalism*

3.3.1 CONVOLUTION FORMALISM AND FERMI MOTION Within the conventional picture of a nucleus as a collection of bound nucleons, it is quite natural to take into account the effects of Fermi motion and nuclear binding. Before the discovery of the EMC effect, the nuclear binding effect was thought to be quite subtle because of its smallness (with typical binding scales of the order of 10 MeV) compared with the energy transfer ν (of the order of several GeV) deposited by lepton scattering in the deep-inelastic region.

The effect of Fermi motion on the structure function of the deuteron was first studied by West (66) and by Atwood & West (67) in the early 1970s. Bodek & Ritchie (68) also investigated this effect and proposed a direct generalization of the incoherent impulse approximation given in the approach of Atwood & West. Bodek & Ritchie described the tensor function of a target nucleus $W_{\mu\nu}^A$

in DIS using a convolution of the tensor $W^N_{\mu\nu}$ of the off-shell nucleon with its momentum distribution $|\phi(k)|^2$ in the nucleus. They used the kinematics of Figure 2 for nuclear DIS, in which a nucleon with momentum lower than the Fermi momentum ($k < k_F$) recoils against the A-1 residual nucleus. In contrast, a nucleon with high momentum ($k \gtrsim k_F$) recoils against another nucleon with which the struck nucleon formed a pair as a result of short-range correlations in the nucleus. (This process is sometimes called the quasideuteron picture.) Essential to this approach is the assumption that all debris in the final state are in their ground, on-mass-shell state. Saito & Uchiyama (69) have further investigated this method using phenomenological momentum distributions.

An important objection to using a momentum distribution with a high-momentum tail in combination with the convolution formalism can nonetheless be raised. In a nucleus, the nucleon four-momentum squared, k^2, becomes negative for large enough $|\mathbf{k}|$, say above ~ 1 GeV, which leads to nonconservation of the normalization of the momentum distribution (70, 71, 72). Certainly,

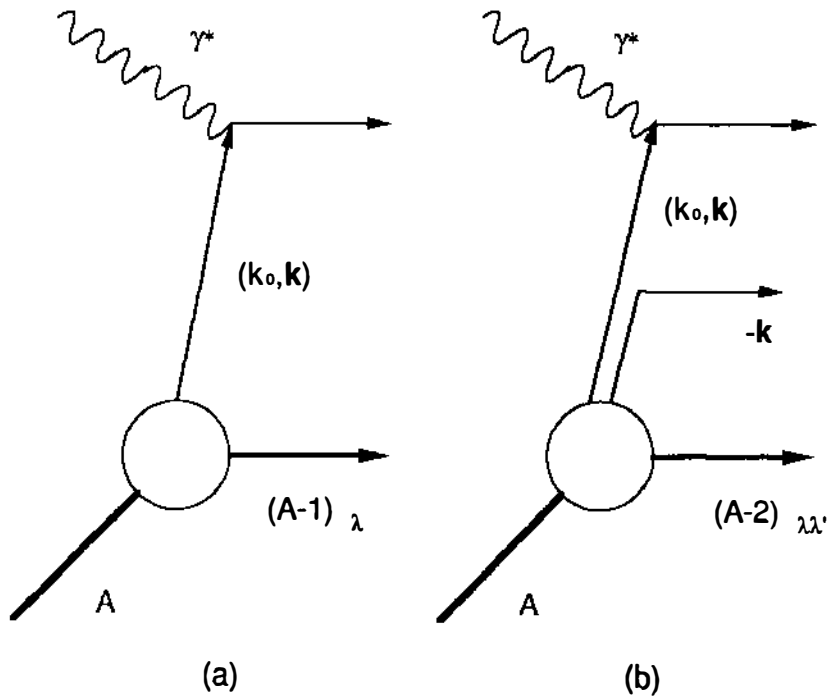

Figure 2 Kinematics for nuclear deep-inelastic scattering: (*a*) $k < k_F$ and (*b*) $k > k_F$.

how the nonrelativistic picture could work for such high $|\mathbf{k}|$ is not at all clear. Frankfurt & Strikman (70) proposed an alternative normalization for the momentum distribution, and Morley & Schmidt (73) discussed nuclear structure functions using a parametrization of relativistic vertex functions instead of nonrelativistic wavefunctions.

Most authors accept the impulse approximation, namely that the off-shell nucleon structure functions appearing in the convolution formalism can be identified with the on-shell functions at some appropriate kinematics. We discuss this approximation in more detail in Section 5.2. This assumption was also used in other attempts to derive a convolution formula [see e.g. Jaffe (74) and Jung & Miller (75)].

3.3.2 NUCLEAR BINDING The importance of the nuclear binding to describe the whole EMC effect was first pointed out by Akulinichev et al (76) and by Dunne & Thomas (77). [Initially, the depletion of the momentum fraction of valence quarks was suggested by Jaffe (78) and by Llewellyn Smith (79). This process is known as x rescaling (see also 58, 80, and 81)].

The separation (or removal) energy ϵ_λ of the struck nucleon in the orbital specified by λ in the nucleus is defined by

$$\epsilon_\lambda = M_A - M^\lambda_{A-1} - M_N, \qquad 47.$$

where M_A is the mass of the target nucleus and M^λ_{A-1} is the mass of the residual nucleus, which is usually in a highly excited hole state, say $(A-1)_\lambda$ (see Figure 2*a*). The nucleon then has the initial energy

$$p_0 = M_N + \epsilon_\lambda - T_R, \qquad 48.$$

where T_R is the recoil kinetic energy of the $(A-1)$ nucleus. This recoil contribution is very important for light nuclear targets (68, 77, 82) but negligible for medium and heavy nuclei. If the quasideuteron picture is chosen to describe the high-momentum components, then the contribution of the recoil term may again be sizeable even for large nuclei (69, 83).

Using the convolution formalism, one can describe the nuclear structure functions in two different ways, e.g. with instant-form dynamics (IFD) (74–77) and with light-front dynamics (LFD) (84, 85). A formalism in IFD is constructed under the subgroup of kinematic Lorentz transformations in which the hyperplane $\xi^0 = t = 0$ is invariant, while LFD requires the subgroup in which the light front, $n \cdot \xi = t + \mathbf{n} \cdot \xi = \xi^+ = 0$, is invariant [$n = (1, -\mathbf{n})$ and $\mathbf{n}^2 = 1$].

In IFD, the nuclear structure function $F_2^A(x)$ is given as a convolution of the free nucleon structure function F_2^N with the momentum distribution $f_\lambda(y)$ for

the nucleon in the λth orbit:

$$F_2^A(x) = \sum_\lambda \int_x^{M_A/M_N} dy f_\lambda(y) F_2^N\left(\frac{x}{y}\right), \quad 49.$$

where y is the momentum fraction carried by the nucleon, and

$$f_\lambda(y) = \int d^4k\, \delta\left(y - \frac{Ak^+}{M_A}\right)\left(1 + \frac{k^3}{k^0}\right) S_\lambda(k), \quad 50.$$

where $k^+ = k^0 + k^3$. The nucleon spectral function is

$$S_\lambda(k) = |\phi_\lambda(\mathbf{k})|^2\, \delta\left(k^0 - M_N - \epsilon_\lambda + T_R\right), \quad 51.$$

and the target nucleus is assumed to be at rest. The factor $(1 + k^3/k^0)$ in Equation 50 is the so-called flux factor. This factor was initially pointed out by Frankfurt & Strikman (70), in combination with the charge conservation condition, and was further investigated by Jung & Miller (75), by Bickerstaff (86), and by Anisovich et al (87). [The flux factor was omitted in the works of Akulinichev et al (76), Dunne & Thomas (77), Birbrair et al (81), and Uchiyama & Saito (82).] If one uses a separation energy $\langle \epsilon_A \rangle$ averaged over all occupied shells and an average momentum distribution of the nucleon $\varphi(|\mathbf{k}|)$, then the y distribution of the nucleon becomes

$$f(y) = \left\langle \sum_\lambda f_\lambda(y) \right\rangle_{av} = \int d^4k \delta\left(y - \frac{Ak^+}{M_A}\right) \left(1 + \frac{k^3}{k^0}\right) |\varphi(\mathbf{k})|^2 \delta\left(k^0 - M_N - \langle \epsilon_A \rangle + \langle T_R \rangle\right), \quad 52.$$

where $\langle T_R \rangle$ is the average value of the recoil kinetic energy.

The main issue in this equation is determining the value of $\langle \epsilon_A \rangle$. First, Akulinichev et al (76) proposed that $\langle \epsilon_{Fe} \rangle = -39$ MeV for iron, using the Koltun sum rule (88). However, this rule seems irrelevant because it is badly violated (89). Dunne & Thomas (77) then used the harmonic oscillator wavefunction for each level, fitted to measured separation energies, to obtain a value of -26 MeV for $\langle \epsilon_{Fe} \rangle$. Li et al (90) presented Hartree-Fock calculations of the EMC ratios for various nuclei using a density-dependent Skyrme force [cf Birbrair et al (81)]. This approach yielded a value of about 26 MeV. These authors also found that the nuclear binding and Fermi motion corrections in the convolution model, with the flux factor, account for only about 20% of the EMC effect in the mid-x region. To correct this discrepancy, Dunne & Thomas (77) proposed a shift of Q^2 because of the off-shell behavior of the nucleon structure function, which was mathematically identical to the dynamical rescaling model but quite different in origin.

In LFD, the nuclear structure function is again given by the convolution form (see Equation 49). However, the average y distribution of the nucleon, $f(y)$, is defined in terms of light-front three vectors, $\tilde{\mathbf{k}} = (k^+, \mathbf{k}_\perp)$ (84, 85, 91):

$$f(y) = \int d^3\tilde{\mathbf{k}}\,\delta\left(y - \frac{Ak^+}{P_A^+}\right)\rho_N(\tilde{\mathbf{k}}), \qquad 53.$$

where P_A^+ is the +-component of the initial momentum of the nucleus and ρ_N is the light-front momentum density defined by

$$\rho_N(\tilde{\mathbf{k}}) = \frac{1}{2}\int dk^- \frac{Ak^+}{P_A^+} S_N(k), \qquad 54.$$

where $S_N(k)$ is the nucleon spectral function. Oelfke et al (91) have discussed the validity of this formalism compared with the IFD and have carefully investigated the three-nucleon system as a test case.

Clearly, theoretical challenges, such as developing off-shell treatments for nucleons and other ingredients, remain that are associated with relativistic bound states. Jaffe (92) and Hoodboy & Jaffe (93) questioned the validity of any convolution formula such as Equation 49. Spit et al (94, 95) and Gurvitz & Rinat (96) have also discussed this problem.

3.3.3 THE PION MODEL A nucleus consists of nucleons bound by the exchange of mesons—mostly pions at intermediate and long range. Because they are bound by mesons, the nucleons do not carry all of the momentum of the nucleus. The whole momentum is shared between the nucleons and (mainly) the pions. When Llewellyn Smith (79) discussed the depletion of valence quarks in a nucleus, he suggested that an increase of virtual pions in the nuclear medium would lead to an enhancement of the EMC ratio at small x. Ericson & Thomas (97) calculated the change of the pion field in a nucleus using the Sullivan formula (98) and the nuclear spin-isospin response function (99). Later, Berger et al (84) and Berger & Coester (85) examined the same idea using light-front dynamics.

We briefly review the calculation of Ericson & Thomas in order to make clear the connection with recent measurements of the nuclear longitudinal response (see Section 5.3). If the nucleus is treated in a simple Fermi gas model with Fermi momentum k_F (as a first-order approximation), the pion contribution to the nuclear structure function in the Bjorken limit may be given by the usual convolution formula with the structure function of the free pion, $F_2^\pi(x)$,

$$\delta^\pi F_2^A(x) = \int_x^1 dy\left[f_\pi^A(y) - f_\pi^N(y)\right]F_2^\pi\left(\frac{x}{y}\right), \qquad 55.$$

where $f_\pi^N(y)$ is the distribution of pions in the free nucleon and $f_\pi^A(y)$ given by:

$$f_\pi^A(y) = \frac{3g^2}{16\pi^2} y \int_{M_N^2 y^2}^{\infty} dq^2 \int_0^{q - M_N y} d\omega \frac{q^2 |G_{\pi NN}(q^2)|^2}{(t + m_\pi^2)^2} R(q, \omega). \qquad 56.$$

Here t is minus the four-momentum squared of the exchanged pion, $q = |\mathbf{q}|$, and $G_{\pi NN}(q^2)$ is the form factor at the $NN\pi$ vertex with the coupling constant g. $R(q, \omega)$ is the nuclear spin-isospin response function [see e.g. Oset et al (99)] in the random-phase approximation (RPA):

$$R(q, \omega) = -\frac{6\pi M_N^2}{g^2 q^2 k_F^3 G_{\pi NN}^2(q^2)} \mathrm{Im} \left[\frac{\Pi^0(q, \omega)}{1 - \left(g' - \frac{q^2}{t + m_\pi^2} \right) \Pi^0(q, \omega)} \right], \qquad 57.$$

where $\Pi^0(q, \omega)$ is the self-energy of the pion arising from nucleon-hole and $\Delta(1232)$-hole excitations and g' is the so-called Landau-Migdal parameter. This mechanism gives a very strong attraction, and the strength can be simply controlled by g'. Using a reasonable value of g', Ericson & Thomas (97) fitted the large enhancement at small x in the original EMC data (1). It is now clear that this enhancement at small x was too high, although almost any level of enhancement can be understood given the present knowledge of g'.

The data taken by SLAC experiments and the Bologna-CERN-Dubna-Munich-Saclay collaboration showed that the EMC ratio has a little bump around $x \sim 0.15$ and falls below unity at very small x because of shadowing (see again Figure 1). Some experiments have been performed and many theoretical discussions have been presented concerning the pion field in nuclei have been performed [see e.g. Abramowicz et al (100), Carey et al (101), Cooper et al (102), Parker et al (103), Ericson & Thomas (104), Esbensen et al (105), Bickerstaff et al (106), Chanfray (107), Birbair et al (108), Epele (109), and Umnikov et al (110)]. We discuss some very recent results of these experiments in Section 5.3. However, further experimental tests are still required to determine whether the pion field in a nucleus is enhanced.

3.4 *Nuclear Shadowing*

Nikolaev & Zakharov (111) initially predicted shadowing and antishadowing effects in nuclear structure functions that they believed were associated with the overlap of partons in different nucleons. [The hadronic properties of the photon were discussed at the end of the 1960s by Gribov (112) and in the pre-QCD era by Bauer et al (113); for a recent review see O'Connell et al (114).] Later, Gribov et al (115) and Levin & Ryskin (116) proposed that the recombination of gluons would screen the rapid increase of the parton density at small x. Since the discovery of the shadowing effect in the EMC ratio (see Figures 1, 3, and

4), many authors have studied nuclear structure functions for small x. Because the shadowing persists even at $Q^2 \sim$ a few GeV^2, both the hadronic (vector meson dominated) and the quark-parton pictures would be needed to describe it. (The old idea connecting two such pictures is given in Reference 117.)

In the parton model, nuclear shadowing results when small-x gluons from different nucleons overlap in the longitudinal direction (118, 119). One can therefore imagine that the shadowing begins when the gluons exceed a longitudinal size comparable to the nucleon-nucleon separation in the nucleus: $x < x_{\text{onset}}$. The shadowing becomes stronger as x decreases and finally reaches a saturation value at $x_{\text{sat}} \simeq 1/2R_A M_N$, where R_A is the nuclear radius. Therefore, nuclear shadowing is associated with two basic distance scales: x_{onset} and x_{sat}. Interestingly, the data show a definite A-dependence (see Figures 3 and 4 and Section 4.7, below). The crossover points and the depth at very small x ($\lesssim 10^{-3}$) depend on the mass number of the target. The crossover point around $x \sim 0.1$ characterizes a typical momentum fraction associated with the onset scale of the shadowing, while the depth is related to the saturation value of the shadowing, which corresponds to that observed in real photon reactions. The argument given above was also discussed by Berger & Qiu (120) and Close & Roberts (121). Close et al (122) have investigated a modification to nuclear structure functions resulting from the fusion of quarks, antiquarks, and gluons [see also Zhu & Shen (123)].

4. EXPERIMENTAL RESULTS

4.1 *Overview*

Although nuclear targets had been used in DIS experiments since their inception, the only dedicated nuclear studies focused on kinematic regions in which the vector dominance model had been used to predict nuclear effects, which are at low Q^2 for nearly real photons. The realization by the EMC collaboration that their iron data differed from their deuterium data had a dramatic effect on the conventional view of nuclear structure and led to an explosion of theoretical and experimental activity. Table 1 gives a selected compilation of the experimental literature of the past decade.

The kinematics of each measurement are defined by the incident beam energy, the statistics of the cross section, and the trigger acceptance of the apparatus. In small acceptance experiments such as the SLAC spectrometer measurements, measurements at different kinematics are relatively decoupled. However, in the lower-luminosity, large-acceptance muon experiments, the kinematic distributions are strongly coupled. Equation 4 clearly shows that $d^2\sigma/dx dQ^2$ is almost independent (to factors of 2) of beam energy and is weighted by $1/(xQ^4)$. Thus

Table 1 Summary of major experimental results

Laboratory/ collaboration	Beam	Energy (GeV)	Measurement	Target	Reference	Year
SLAC E139	e	8-24.5	σ	D, ^{4}He, Be, C, Ca, Fe, Ag, Au	(2, 124)	1994, 1984
SLAC NE-11		1.5–9.8	νW_2, R $x \sim 1$	Al	(125)	1992
SLAC E140		3.75–19.5	R_a-R_b, σ_a/σ_b	D, Fe, Au	(3, 9)	1988
SLAC		8–24.5	σ	H, D	(126, 127)	1992, 1990
CERN NMC	■	90,280	σ	H, D	(128)	1992
		90,280	ΔR	D to H, Ca to C	(129)	1992
		90	σ_A/σ_{Li}	^{6}Li, ^{12}C, ^{40}Ca	(130)	1992
		200,280	$\sigma_{J/\psi}$	Sn/C	(131)	1991
		200	σ_A/σ_D	D, ^{4}He, C, Ca	(132)	1991
		90–280	σ_D/σ_H	D, H	(133)	1991
		90–280	σ_D/σ_H	D, H	(134)	1994
CERN BCDMS	μ	200	$\sigma_C(x \sim 1)$	C	(135)	1994
		120,200,280	σ_D, σ_H	H, D	(136)	1990
		200	σ_A/σ_D	Fe, D	(4)	1987
		120,200,280	σ_C, R	C	(137)	1987
		280	σ_A/σ_D	D, N, Fe	(138)	1985
CERN EMC	μ	100–280	σ_A/σ_D	Cu, D	(5)	1993
		280	σ_A/σ_D	D, C, Ca	(139)	1988
		100–280	σ_A/σ_D	D, C, Cu, Sn	(6)	1988
		280	σ_A/σ_D	H, D, Fe	(140)	1987
		120–280	σ_A	Fe	(141)	1986
		100–280	σ_A/σ_D	D, Fe	(1)	1983
FNAL E665	■	490	Final State	D, Xe	(142)	1995
		490	Final State	D, Xe	(143)	1994
		470	σ_D/σ_H	H, D	(144)	1995
		490	σ_A/σ_D	D, Xe	(145)	1992
		490	σ_A/σ_D	D, Xe	(146)	1992

at each value of x, there is a strong statistical weighting of the lowest Q^2 accepted by the experimental trigger. However, there is generally a minimum energy loss for which the apparatus performs acceptably. Accordingly, there is an almost linear relation between average x and Q^2. This relation can in turn occasionally cause conclusions that appear obvious from one-parameter distributions in x and Q^2 to be altered, i.e. an apparent dependence on x is seen to be a Q^2 dependence in more complete data. An excellent compilation of structure functions, including results of A-dependence, was recently published (147). (At this writing, the data can be accessed in the Durham/RAL HEP database via World Wide Web at http://cpt1.dur.ac.uk/HEPDATA.)

4.1.1 RADIATIVE CORRECTIONS Radiative corrections are both the glory and the curse of electromagnetic probes. They are important because the lepton and photon propagators lead to a strong dependence of the experimental cross sections on the kinematic variables. For example, in an experiment that detects only the outgoing lepton, one cannot distinguish a high Q^2 one-photon-exchange event with large ν from a class of lower Q^2 events in which an extra photon is radiated. The larger cross section at lower Q^2 can partially compensate for the extra power of α_{em} involved in the radiative event. With electromagnetic probes, these corrections can be accurately, although quite laboriously, calculated. Two theoretical analyses of radiative corrections have been extensively employed in DIS experiments. Most of the earlier work is based on the formalism of Mo and Tsai (148, 149). An alternative formalism, which does not introduce an artificial division in the infrared dependence, has been developed at Dubna by Akhundov et al (150–152). Studies have shown that if the same physics is included, the numerical results of the two formalisms are the same to the 1–2% level (153). However, our changing understanding of the physics inputs, which has led us to include the τ lepton and the quarks in the loop corrections, for example, together with better parameterizations of the single photon cross sections in a wide range of Q^2 and ν, has made the results somewhat time dependent.

The primary nuclear dependence in the radiative corrections arises from bremsstrahlung, in particular from coherent radiation of a photon in nuclear elastic scattering or quasifree scattering from a nucleon. Both cross sections are large at low Q^2. The nuclear structure functions introduce only a weak nuclear dependence for the inelastic radiative events. Many of the corrections, such as the vertex and fermion loop corrections, cancel in the ratio of nucleus to deuterium cross sections. Since neutrino scattering does not have such a strong dependence on Q^2, the radiative corrections are considerably less important in neutrino interactions than they are in the electromagnetic case. At very low values of x, say $x < 0.001$, radiative processes can become equal to or much larger than the single photon cross section. Using information on the

final-state particles, obtained by direct detection of either the bremsstrahlung photons or the multiple hadrons from an inelastic scattering, one can push the measurements to extremely low x ($\sim$ 0.00002) but with a rather different set of systematic uncertainties.

4.1.2 SLAC The Stanford Linear Accelerator Center produced the pioneering work on DIS in 1967 and led the field until the quest for higher energies and higher momentum transfer led investigators to concentrate on muon and neutrino beams. Early studies of scattering from nuclei are reported in References 144 and 145. In many ways, the SLAC experiments are textbook examples of scattering measurements and are generally the simplest in which to understand the systematic errors. The incident e^- beam has a well-measured energy, with a narrow beam phase space, and is very intense (10^{14} e^-/s). With typical target thicknesses limited by the size of the radiative corrections (a few percent of the radiation length), luminosities of 10^{38} electron-nucleons/cm^{2}s are routinely obtainable, enabling repeated measurements of the same point in studies of the systematics. The detectors are small-solid-angle magnetic spectrometers, with geometrical apertures of modest size that define the acceptance, and highly efficient detector systems. With these attributes, the SLAC experiments have become the standard for absolute cross-section measurements, and coupled with the easy variability of the beam energy, are a prime source of information on the photon polarization dependence (R) of the cross section.

With the first announcement of the EMC results, Bodek et al (156, 157) were able to add important new information. Systematic studies of the A-dependence of the cross sections and the A-dependence of the longitudinal-transverse ratio $R(\equiv \sigma_L/\sigma_T)$ were begun immediately. The recent extension of the SLAC energy to 50 GeV has led to renewed possibilities for measurements in the future at lower values of x. At the other extreme, the availability of lower energies, which is enhanced by the construction of the SLAC Nuclear Physics Injector, makes SLAC a primary source of information on nuclear structure functions at $x > 1$.

4.1.3 MUON EXPERIMENTS Muon beams for DIS were driven by the quest for higher Q^2. A muon beam is a tertiary beam produced at a high-intensity proton accelerator by collecting a limited phase-space beam of pions and kaons that partially decay to muons and by filtering out the remaining hadrons with an absorber. The process produces a beam with a broad phase space, with particles of energy distributed up to 5–20% from the central value and a primary spot size at the target of several centimeters in transverse extent with a considerable halo extending meters away from the target. Each individual muon must be tracked

in order to define its energy and trajectory precisely (0.1–0.5%). The need for tracking of the beam particles limits the allowable luminosity, which usually ranges from 10^6 to a few times 10^7 muons/s, depending on the fraction of the energy of the primary proton beam desired for the muons. One compensating factor is that the bremsstrahlung cross sections are reduced by $(m_e^2)/(m_\mu^2)$, allowing targets of about one radiation length. The overall luminosity can then be $\sim 10^{33}$ muon-nucleons/cm^{2}s, and a high statistics measurement requires large acceptance for the scattered muons. This acceptance is advantageous in that it simultaneously can be made efficient for the hadronic final state, although at the cost of increased complexity and some additional loss of luminosity (reduced target thickness), to limit hadronic reinteractions in the target material.

4.1.4 EUROPEAN MUON COLLABORATION The EMC did not start out to measure the nuclear dependence of DIS but simply to increase its luminosity by using a denser target material. Because the EMC measured absolute cross sections, when they compared their iron results to deuterium results from a different period of beam, the differences were meaningful, but with a substantial (7% in the absolute magnitude and up to 30% in the slope vs x) systematic error band (1). Systematic differences have been noted between the absolute structure functions published by the EMC and those of SLAC, BCDMS, and the New Muon Collaboration (NMC). The measurements of the last three groups generally agree well in regions of overlap. In subsequent EMC measurements, the deuterium and nuclear targets were interchanged (6), or deuterium and nuclear targets were run simultaneously (5, 139), which substantially reduced the systematic errors. In various configurations, the EMC has performed the most extensive studies of the distributions of outgoing hadrons following DIS, in part with nuclear targets (158–160).

4.1.5 BCDMS The BCDMS collaboration also concentrated on high-luminosity measurements of absolute structure functions. The relatively homogeneous and cylindrically symmetric structure of their apparatus simplifies the understanding of systematic effects. Most of the BCDMS data are from separate running on hydrogen, deuterium, and carbon targets; however, in respective dedicated experiments, deuterium, nitrogen, and iron (138) and deuterium and iron (4) were measured simultaneously.

4.1.6 NMC The NMC took over the EMC apparatus and upgraded it to improve the muon tracking efficiencies. This group has made the most elegant attempt to eliminate A-dependent systematic errors by measuring with deuterium and nuclear targets simultaneously and by frequently interchanging the locations of the target sets. This approach yields a measurement of the ratio of cross

sections that is almost independent of the spectrometer acceptance and of the counting of beam particles.

4.1.7 FNAL E665 E665 used the higher beam energy available at Fermilab to extend the range of x and W in DIS with large acceptance detection of the final state. In the first measurements, the target was contained in a streamer chamber, and separate running on hydrogen, deuterium, and xenon targets led to substantial ($\sim 7\%$) relative systematic errors. In later measurements, the targets were changed every few minutes, and the resulting systematic errors on the cross section ratios were at the 1–3% level. In the region of $W > 20$ GeV, corrections to the parton model are explicitly seen in the jet structure of the hadronic final state (161). E665 was also able to control a large fraction of the radiative corrections by directly detecting the radiated photons in its large electromagnetic calorimeter. This capability permitted measurements at extremely low x values corresponding, as defined by the kinematics, to very low values of Q^2.

4.1.8 NEUTRINO SCATTERING The neutrino measurements are generally absolute structure function measurements on single or composite targets: Fe-CDHSW (162); H,D-BEBC (163–165); Ne-BEBC (166); and Fe-CCFR (167, 168). The energy of the unmeasured beam neutrino is deduced from calorimetric information on the hadronic final state. Since the mass of the W boson is large, the cross sections do not have a strong dependence on Q^2, and poorer kinematic resolution can be tolerated. Kitagaki et al (169) have studied the dependence of the structure function on the presence of slow protons in the interaction vertex, but the appearance of slow protons does not seem to be directly related to the EMC effect (170–172). The BEBC collaboration has published one study of the ratio of neon to deuterium in the low x shadowing region (173).

4.2 *A-Dependence of Nuclear Cross Sections*

Figure 1 illustrates the x dependence of the ratio of combined iron and copper data to deuterium, while Figure 3 displays the landscape of the A-dependence on a logarithmic scale in x for carbon and calcium data. The lowest x data available are those on xenon. Figure 4 shows the combined tin, xenon, and silver data. In each case, the cross-section ratio is plotted for the nuclear target vs deuterium, which is assumed to be the sum of the neutron and proton cross sections. (This assumption is discussed further in Section 4.7.) This presentation of data is based on two explicit assumptions: (*a*) The ratio of cross sections does not depend on Q^2, and (*b*) R does not depend on the target. Both of these assumptions are discussed in more detail below. Sick & Day (174) have extrapolated the experimental results to nuclear matter using the local density approximation and an $A^{1/3}$ power law dependence at each x.

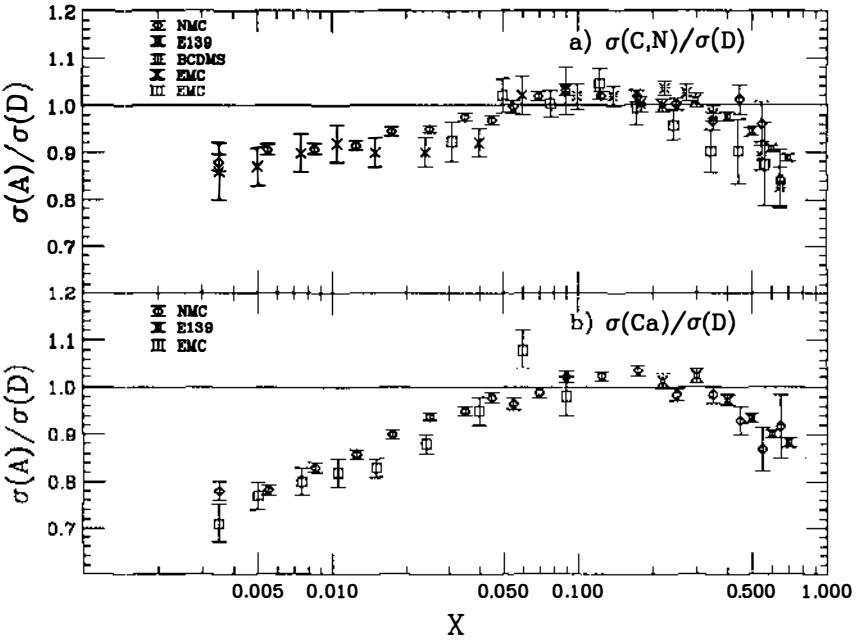

Figure 3 Ratios of the deep inelastic cross section on targets of (*a*) carbon and nitrogen and (*b*) calcium to those of deuterium (2, 6, 132, 138, 139).

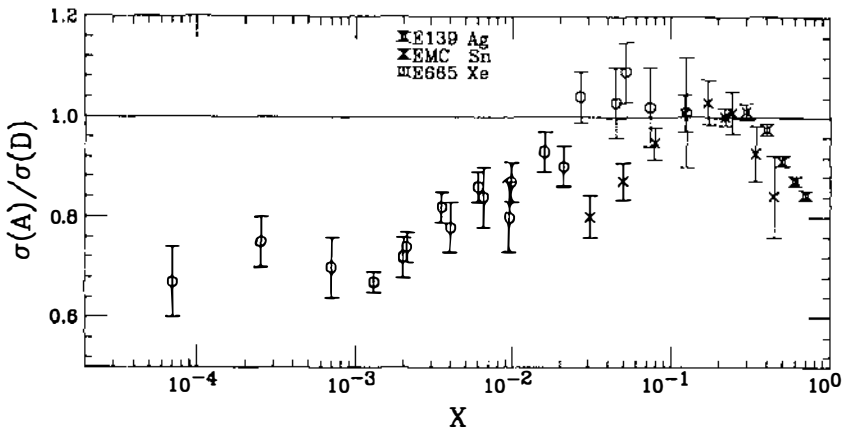

Figure 4 Ratios of the deep-inelastic cross section on targets of tin, xenon, and silver to those of deuterium (2, 6, 145, 146).

4.3 *The Behavior of* σ_L/σ_T *with x and A*

To the extent that partons are pointlike spin-1/2 particles, the absorption cross section of a longitudinal photon should be much smaller than that of a transverse photon ($\sim 4m_q^2/Q^2$, where m_q is the parton mass), resulting in a ratio $R(\equiv \sigma_L/\sigma_T)$ close to zero. This prediction was an early success of the quark-parton model. Two mechanisms that generate longitudinal cross sections for the nucleon are the intrinsic transverse momentum of the partons, $\mathbf{k}_T$, which adds to the effective mass [$R \sim 4(m_q^2 + \mathbf{k}_T^2)/Q^2$], and the contribution at the next order in α_s from the gluon distribution:

$$F_L(x, Q^2) = \frac{\alpha_s(Q^2)}{2\pi} \int_x^1 \left[\frac{8}{3} F_2(z, Q^2) + \frac{40}{9}\left(1 - \frac{x}{z}\right) z G(z, Q^2)\right] \frac{dz}{z^3}. \quad 58.$$

$G(x)$ becomes very large at low x, giving rise to substantial (~ 0.3) R values below $x \sim 0.1$. The most accurate measurements are those of the SLAC groups (3, 175). Whitlow et al (127) have performed a global analysis of the results for $x \geq 0.1$ (a selection of these results is shown in Figure 5) and have parameterized the results with the following form, which is now used in

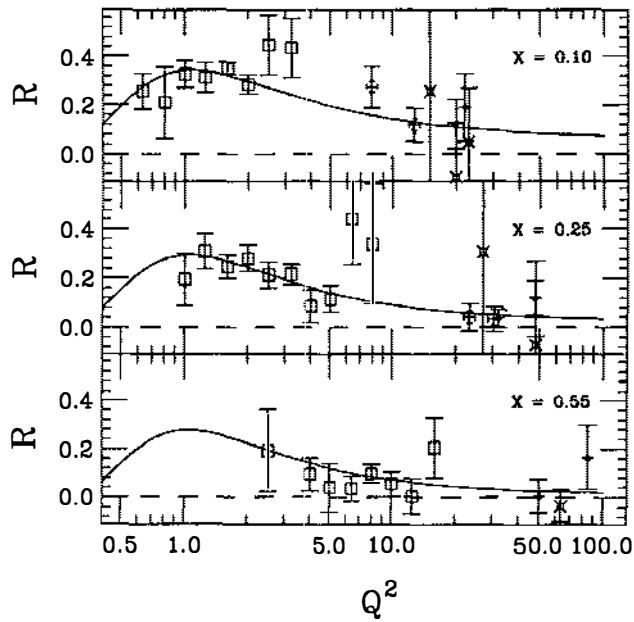

Figure 5 Measurements of $R = \sigma_L/\sigma_T$. The solid curve is the parameterization of Whitlow et al (127).

essentially all analyses:

$$R^{\text{fit}} = \frac{b_1}{\ln(Q^2/\Lambda^2)}\Theta(x, Q^2) + \frac{b_2}{Q^2} + \frac{b_3}{Q^2 + (0.3\ \text{GeV})^2} \quad 59.$$

$$\Theta(x, Q^2) = 1 + 12\frac{Q^2}{(Q^2 + 1\ \text{GeV}^2)}\frac{0.125^2}{(0.125^2 + x^2)}, \quad 60.$$

where $\Lambda = 0.2$ GeV, $b_1 = 0.0635$, $b_2 = 0.5747$, and $b_3 = -0.3534$. [Note that the original reference (127) contained a typographical error in the value of b_1.] The authors are careful to state that this parameterization is not expected to be valid for $Q^2 < 0.3\ \text{GeV}^2$. However, in the absence of other data, many authors use this parameterization over the entire kinematic region, especially in radiative correction calculations that require knowledge of the cross sections in unmeasured regions.

The intrinsic transverse momentum $\mathbf{k}_T$ or the gluon distribution $G(x)$ may be affected by the nuclear environment, and thus R may also be nucleus dependent. In principle, $\mathbf{k}_T$ can also be measured in the azimuthal asymmetry of the final-state hadrons, but no nuclear comparisons are available. All existing measurements are consistent with little nuclear dependence of R in the regions in which it has been measured. The results from SLAC and NMC are summarized in Figure 6. The average of all the SLAC results is $R_D - R_p = -0.001 \pm 0.009 \pm 0.009$. The average of the NMC results is $R_D - R_p = 0.031 \pm 0.016 \pm 0.011$ and $R_{Ca} - R_C = 0.027 \pm 0.026 \pm 0.020$. Therefore, the ratio of cross sections directly measures the ratio of structure functions F_2.

4.4 Q^2 *Dependence of Nuclear Cross Sections*

The Bjorken limit requires large Q^2 to be applicable for two reasons: to precisely define the light-cone direction and to reduce higher-twist contributions in the operator product expansion (OPE). Nuclear structure functions can be directly interpreted as parton distributions only if these conditions are satisfied. The first condition places a restriction on x^2/Q^2 and is usually well satisfied, even at relatively low values of x and Q^2. However, the value of the higher-twist terms is under little theoretical control, and these terms can have specific nuclear dependences. Experimentally, the ratio of nuclear cross sections to deuterium has little detectable dependence on Q^2, as can be seen in Figure 7, which shows the derivative of the cross sections with respect to $\ln Q^2$, combining SLAC, NMC, and BCDMS data for iron and calcium. Over a broader x region, the derivative of the calcium/deuterium cross sections with respect to $\ln Q^2$ is shown in Figure 8. This absence of any observable dependence of the ratio on Q^2 justifies the usual practice of combining all the Q^2 data at a fixed x-value to display the x-dependence of the ratio.

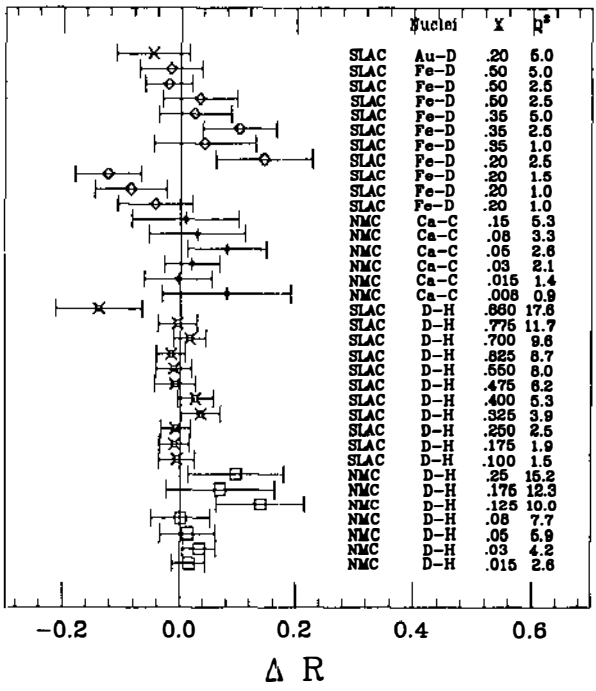

Figure 6 Measurements of the difference in $R = \sigma_L/\sigma_T$ for a variety of targets (3, 129).

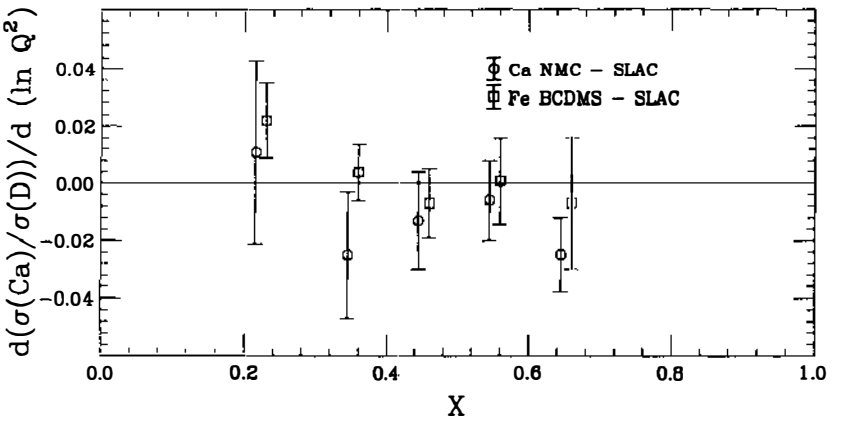

Figure 7 Measurements of the derivative of the ratio of cross sections of calcium and iron to deuterium with respect to ln Q^2 (2, 4, 132).

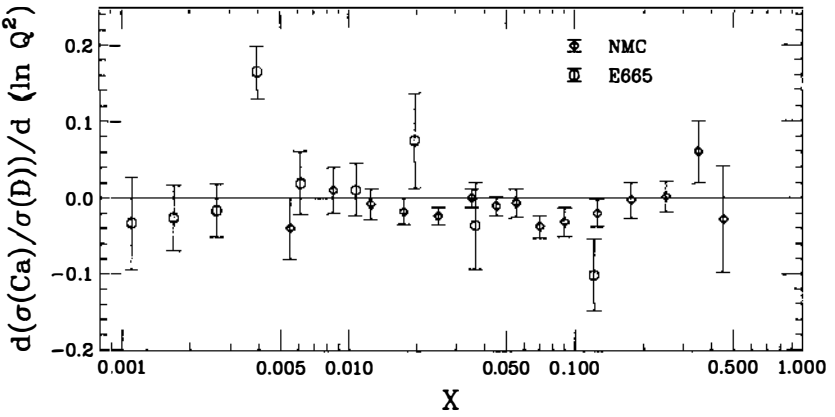

Figure 8 Measurements of the derivative of the ratio of calcium to deuterium cross sections with respect to ln Q^2 over a broad range of x (132, 176).

Many groups have studied whether perturbative QCD can accurately describe the Q^2 dependence of the structure functions. The Q^2 dependence of the hydrogen (177, 178), deuterium (178, 179), carbon (180), and iron data (167) is well reproduced by QCD at large Q^2. The sensitivity to higher twist is parameterized by including a phenomenological $[1 + C(x)/Q^2]$ dependence (128, 181, 182). The results appear to be quite sensitive to the details of the implementation. For example, while one study (181) of the BCDMS and SLAC data indicated that the twist-4 contributions in hydrogen and deuterium were very small at low x, a different analysis of the same data set (182) revealed significant twist-4 terms at low x. The NMC (128) also found small higher-twist contributions at low x. In all analyses, the hydrogen and deuterium higher-twist coefficients become quite sizable for $x > 0.4$ even after inclusion of the so-called target mass correction (183). For example, at $x = 0.8$, the higher-twist contributions are $\sim 20\%$ at Q^2 of 10 GeV^2.

4.5 *A-Dependence of Drell-Yan*

DIS is the most completely analyzed tool for measuring parton distributions, but it is limited to measuring the charge-weighted (either electromagnetic or weak) sum of the parton distributions. The quark-flavor dependence must be addressed in order to separate the contributions from valence quarks and sea quarks. Neutrino scattering is a powerful tool in this regard, but to date, the precision of the identification of nuclear effects is quite limited. The Drell-Yan process, defined as lepton pair production in hadron-nucleus collisions, uses the same elementary diagram as DIS but in the s-channel (i.e. it involves timelike

virtual photons, whereas the t-channel involves spacelike virtual photons). The parton level cross section for the reaction $h + T \rightarrow \gamma_v + X$ is:

$$\sigma_{\mathrm{DY}} = K\frac{4\pi\alpha^2}{9M_\gamma^2}\sum_i e_i^2\left[q_i^h(x_h)\bar{q}_i^T(x_T) + \bar{q}_i^h(x_h)q_i^T(x_T)\right], \qquad 61.$$

where x_h (x_T) is the fraction of the projectile (target) participating momentum carried by the quark. In the simple quark annihilation process, x_h and x_T are determined by the measurement of the virtual photon through its decay into a $\mu^+\mu^-$ or e^+e^- pair. In actuality, the higher-order QCD corrections are significant, approximately doubling the parton-model cross section, hence the K factor in Equation 61. These corrections have now been calculated in considerable detail (184) and are believed to be under control, but the results, which are all based on higher-order calculations, are still renormalization-scheme and scale dependent. The nuclear dependence of these higher-order corrections appears in the parton distributions and in a possible nuclear dependence of the scale and is conjectured to be small.

Choosing a proton projectile and taking x_h to be large (>0.3) causes the reaction to be dominated by valence quarks of the projectile annihilating with sea antiquarks of the target. If the $\bar{u}_T$ distribution is comparable to the $\bar{d}_T$ distribution, then the valence and charge weighting gives eight times the cross section on the $\bar{u}_T$ quarks and provides a very direct measurement of the change of the $\bar{u}_T$ distribution in nuclei.

In FNAL experiment E772 (185), precise measurements were made of the ratio of nuclear Drell-Yan cross sections to deuterium. The results are illustrated in Figure 9. For $x_T > 0.1$, the ratios are consistent with unity, demonstrating that the antiquark distributions in this region are not changed in the nuclear medium. Below $x_T \sim 0.1$, the ratio becomes less than 1.0 on the heavier targets, indicating a reduction of the $\bar{u}_T$ distribution in heavy nuclei, as discussed in Section 3.4. One can also conclude that the excess of the ratio over 1.0 that is observed in DIS (see Figures 1 and 3) near $x \sim 0.15$ must result from an enhancement of the valence quarks.

4.6 *Measurements of the Glue*

Although DIS and Drell-Yan experiments give accurate measurements of the quark distributions, they can provide information on the distribution of the gluons only through α_s corrections and sum rules. The most direct data come from the momentum sum rule:

$$1 = \int_0^1 xG(x)dx + \sum_i \int_0^1 xdx[q_i(x) + \bar{q}_i(x)]. \qquad 62.$$

A more precise definition of the fraction of momentum carried by the quarks, which takes into account target mass effects, is (186, 187):

$$I_S = \int_0^1 F_2(x, Q^2) K_2(x, Q^2) dx \qquad 63.$$

$$\Delta I_S = \int_0^1 \left[\frac{F_2^A}{F_2^D}(x) - 1 + \left(\frac{A M_N}{M_A} - \frac{2M_N}{M_D} \right) \right] K_2(x, Q^2) dx \qquad 64.$$

$$K_2(x, Q^2) = \sqrt{1 + \frac{4M_N^2 x^2}{Q^2}} \left(\frac{2}{1 + \sqrt{1 + \frac{4M_N^2 x^2}{Q^2}}} \right)$$

$$\left(1 - \frac{M_N(\xi)^4}{Q^4} \right) (1 + 3\eta_2). \qquad 65.$$

(Note that I_S differs from the sum of momentum carried by the quarks by a factor of 5/18 because of the electromagnetic charges of the quarks.) ΔI_S measures

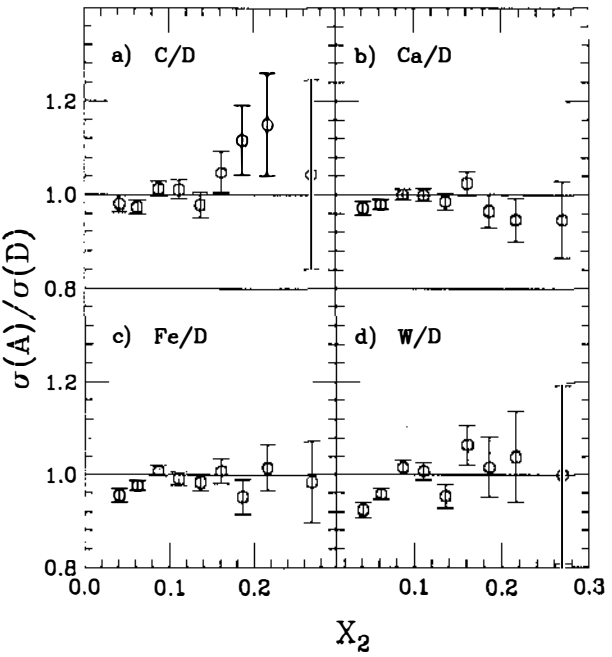

Figure 9 Ratios of the Drell-Yan cross sections on nuclear targets to deuterium (from Reference 185).

Table 2 The integrated quark momentum distribution (I_S) in deuterium and the change in the integrated momentum distribution (ΔI_S) in nuclear targets (132).

Target	x range	Momentum sum	Stat.	Syst.
D	0.–1.	0.148		
He-D	0.0035–0.86	−0.0008	0.0004	0.0022
C-D	0.0035–0.78	−0.0016	0.0007	0.0014
Ca-D	0.0035–0.78	−0.0035	0.0006	0.0014

the difference between I_S in the nucleus of mass A and the deuteron, and K_2 is a correction (near unity) for a more precise definition of the momentum fraction. The mass ratios correct for the average mass change of the bound nucleons. In Table 2 we summarize the nuclear dependence of the integrated quark contribution to the momentum sum rule as determined by the NMC (130). Remarkably, even with the significant x-dependence in the ratios of structure functions between nucleon and nuclear targets, the fraction of momentum carried by the quarks is essentially unchanged in the nucleus.

QCD corrections to the parton model lead to sensitivity to $G(x)$ in many processes. Those studied to date are: (*a*) the longitudinal structure function $F_L(x)$, (*b*) the evolution of the structure functions $dF_2/[d(\ln Q^2)]$, (*c*) heavy-quark production in nuclei, and (*d*) jet production in nuclei.

Equation 58 gave the contribution of the gluon distribution to the longitudinal structure function. The measurements of the A-dependence of R at low x could be used to place limits on possible differences in the gluon distributions. To date, however, no detailed analysis of this kind has been performed.

As discussed in Section 2, the gluon distribution plays a major role in Q^2 evolution of the singlet structure functions. Much of our knowledge of the proton gluon distribution comes from the analysis of this evolution (see e.g. 177, 178). Obviously this technique loses sensitivity for $x > 0.2$, at which point the valence quark distribution dominates. In contrast, at very low x, the gluon distribution almost completely dominates (188):

$$F_L(x, Q^2) = \frac{\alpha_s(Q^2)}{3\pi} \sum_{\text{active flavors}} e_i^2 x G(\xi_L x, Q^2), \qquad 66.$$

$$\frac{\partial 2xF_1(x, Q^2)}{\partial \ln(Q^2)} = \frac{\alpha_s(Q^2)}{3\pi} \sum_{\text{active flavors}} e_i^2 x G(\xi_T x, Q^2), \qquad 67.$$

where ξ_L and ξ_T can be calculated ($\xi_{T,L} \sim 2$) in QCD. The sum is over the active flavors, and important threshold effects occur near the heavy-quark thresholds. From the measurements in Figure 8, an upper limit of $\Delta x G(x) \sim$

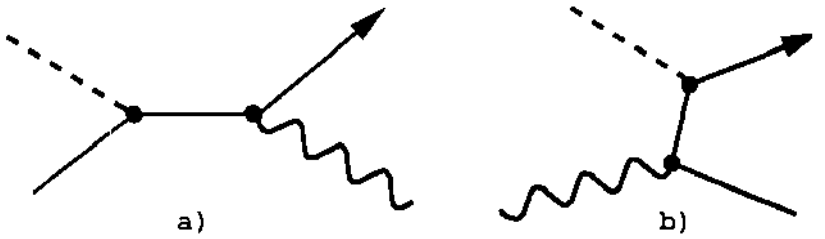

Figure 10 First-order α_s contributions to deep-inelastic scattering. (*a*) Gluon bremsstrahlung, (*b*) photon-gluon fusion.

$.1 \cdot 2\pi F_2/\alpha_s \sim 0.5$ can be set. One must be careful in these comparisons since $\partial[xG(x, Q^2)]/\partial \ln(Q^2)$ is large at low x.

More direct information may be obtained from measurements of the photon-gluon fusion diagram, one of the two next-order diagrams shown in Figure 10 that contribute to DIS. Photon-gluon fusion is believed to be the predominant source of heavy quarks (c, b) in DIS since the intrinsic heavy-quark distributions are expected to be very small and since heavy quarks are only infrequently produced in hadronization.

The NMC (131) has measured the ratio of J/ψ production on carbon and tin targets. The results are shown in Figure 11. The coherent J/ψ production with little excitation of the target must be separated from incoherent, deep-inelastic J/ψ production. The color-singlet model (189) provides a good description of the inelastic J/ψ kinematic distributions. In this model, the ratio of cross sections is used to directly measure the ratio $G_{Sn}(x)/G_C(x) = 1.13 \pm 0.08$ in the vicinity of $x \sim 0.1$. The x of the gluon is given by

$$x = \frac{1}{s}\left[\frac{M^2_{J/\psi}}{z} + \frac{p_t^2}{z(1-z)}\right], \qquad 68.$$

where s is the square of the total energy in the photon-nucleon system and $z = E_{J/\psi}/\nu$ is the laboratory fractional energy of the J/ψ. This measurement suggests that the gluon distribution in the nucleus may be slightly enhanced in the same region as the small enhancement of the quark distributions.

Experiment E665 (190) has presented preliminary results on the ratio of events with two forward jets of hadrons for $0.001 < x < 0.1$ that will enable us to examine the contributions of these QCD processes. A detailed discussion of the intricacies and uncertainties of jet analyses is not appropriate here (see 161). Since almost all higher-order processes are sensitive to collinear and infrared divergences, care must be taken in defining and interpreting these event topology results. However, the A-dependences of the one forward–jet and two forward–

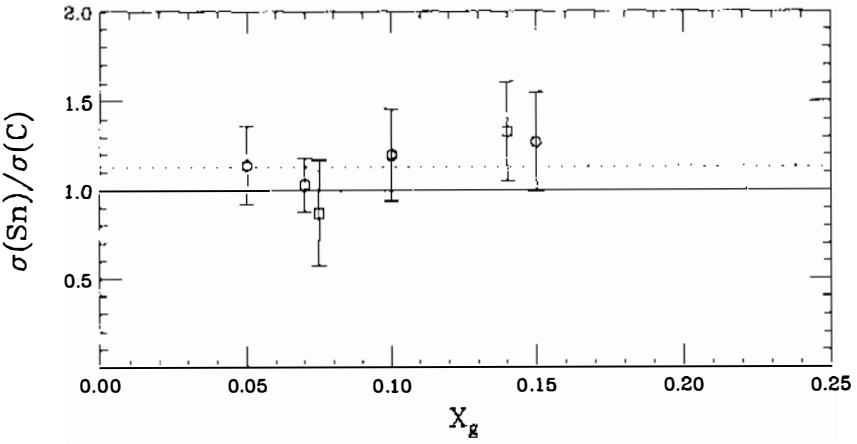

Figure 11 NMC (131) measurements of the ratio of cross sections of J/ψ production on tin and carbon targets.

jet cross sections appear to differ significantly. (Note that the target remnant jet in the backward hemisphere in the center of mass is unobserved.) With further work, this technique may become a valuable measure of the changes in gluon distributions at low x. (See the discussion of shadowing below.)

4.7 *The Shadowing Region*

At low x, the shadowing region, large reductions are observed in the nuclear cross sections compared with the deuterium cross sections. As discussed in Section 3.4, all models of shadowing have two basic longitudinal distance scales related to $1/x$: the "separation between nucleons" (x_{onset}), where interference effects can begin, and the nuclear diameter, which limits the ultimate magnitude of interference. At values of $1/x$ larger than the nuclear diameter, shadowing should saturate (x_{sat}) at a value of the ratio of cross sections corresponding to that observed in real photon reactions. On heavy nuclei such as calcium and xenon, saturation occurs at x values such that the typical $Q^2 \sim 0.1-2\ (\text{GeV}/c)^2$ are comparable to the ρ meson mass squared m_ρ^2. For xenon, the ratio

$$\frac{x_{\text{onset}}}{x_{\text{sat}}} \sim \frac{0.04}{0.002} \sim \frac{11\ \text{fm}}{R_{NN}} \qquad 69.$$

corresponds to $R_{NN} \sim 0.5$ fm. Note that the measured value of x_{sat} is somewhat lower than the simple estimate of $1/2R_A M_N$ given in Section 3.4. Several mechanisms probably conspire to produce the slight excess around $x \sim 0.15$, so that only the general scale found in Equation 69 is relevant. The A-dependence of the

cross section in the saturation region, $A^{0.9}$, agrees with that observed for photon total cross sections, although the ratio of cross sections appears to be slightly larger for all the deep-inelastic data than that obtained by extrapolating the real photon total cross sections of Reference 191 to comparable photon energies.

Recent data from the NMC and E665 show clear evidence of shadowing even in the lightest nucleus, the deuteron. This finding is illustrated in Figure 12. The calculations of References 192 and 193 give a good description of this shadowing. Therefore, any extraction of the neutron structure function must use a model to separate the nuclear effects. In particular, the Gottfried sum can be used to extract the integrated difference in the $\bar{u}$ and $\bar{d}$ distributions:

$$S_G = \int_0^1 \frac{F_2^p(x) - F_2^n(x)}{x} dx = \frac{1}{3} + \frac{2}{3} \int_0^1 [\bar{u}(x) - \bar{d}(x)] dx. \qquad 70.$$

If $F_2^n(x)$ is taken to be $2F_2^D(x) - F_2^p(x)$, as is usually done, then shadowing tends to artificially reduce the extracted $F_2^n(x)$ and increase the apparent value of S_G. Using x_{sat} of xenon as a scale, one might expect saturation of shadowing in deuterium at $x \sim 0.008$. Badelek & Kwiecinski (192) estimate that the NMC result (134) of $S_G = 0.235 \pm 0.026$ should be reduced by 12% because of shadowing, while Melnitchouk & Thomas (193) find a reduction between 4 and 10% when meson-exchange contributions are included.

The various models for shadowing all give comparable predictions for the inclusive scattering cross sections because they basically depend on the two physical length scales discussed above, even though they seem to represent quite different physical pictures. In classic vector-meson dominance descriptions,

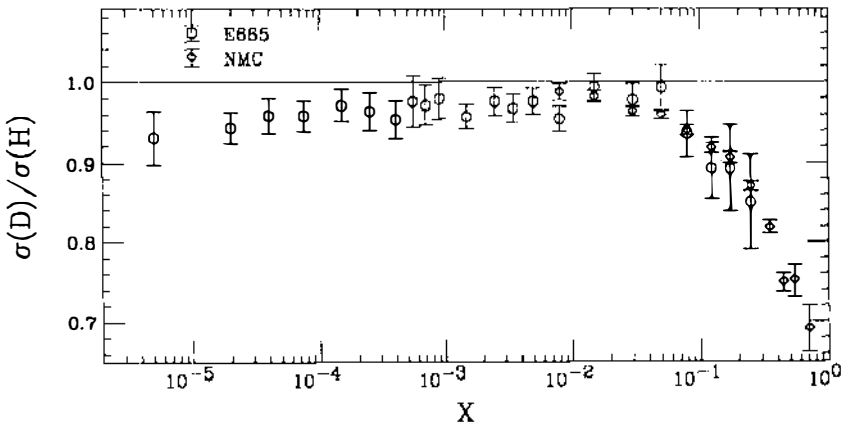

Figure 12 Ratio of deuterium to hydrogen cross sections (134, 144).

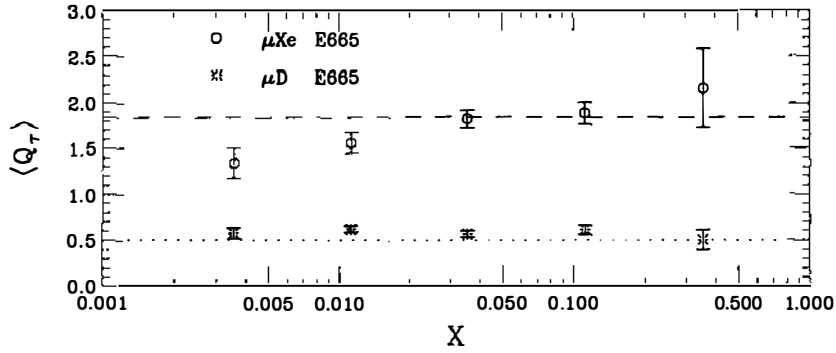

Figure 13 Average net charge in 490-GeV muon-deuterium and muon-xenon interactions (142). The lines at 0.5 and 1.82 simply illustrate average behavior that would be independent of x.

shadowing appears to be a loss of incident flux through the nucleus, although a more careful examination reveals that it arises through interference between single and double scattering contributions. This interference appears to be a volume effect as is the partonic recombination description of a change in the parton density distributions. One way to disentangle these mechanisms may be to examine the hadronic final states. If shadowing is due to interactions on the nuclear surface, then the associated hadronic debris that goes forward in the laboratory frame will have to pass through more nuclear material on average than if the scattering takes place approximately uniformly throughout the nuclear volume. One of the most direct indications of the extent of reinteraction is the total charge in the hadronic final state. At low x, where the cross sections of the virtual photon on the proton and neutron are almost equal, the average charge from the photon interaction is simply Z/A. Subsequent collisions with nuclear protons will increase the average charge

$$\langle Q \rangle = \frac{Z}{A} \langle \nu_C \rangle, \qquad 71.$$

where $\langle \nu_C \rangle$ is the average total number of interactions, including that of the virtual photon. Figure 13 shows the results of measurements of the average charge on deuterium and xenon (142). Remarkably, the number of collisions appears to decrease at low x, in contrast to the simple surface reaction expectation. Similar trends can be seen in other measurements of nuclear reinteraction (142, 194), such as measurements of the number of preequilibrium protons (200 MeV/c < proton momentum < 600 MeV/c), of the total charged-particle multiplicity in the backwards hemisphere of the center of mass, and of the multiplicity of thermal neutrons (1–10 MeV).

This reduction in the reinteractions of the hadronic debris can be explained by the appearance of a class of events with few reinteracting slow hadrons. The slow hadrons in the target fragmentation region are usually thought to result from the hadronization of the color flux tube connecting the struck quark with the diquark remnant. Events with no slow hadrons are likely to be DIS events that do not involve large color separations, i.e. diffractive events with large gaps in rapidity between the target and the slowest detected hadrons. The importance of diffractive events at low x in $e-p$ scattering has been clearly demonstrated at HERA (195). Figure 14 shows the E665 measurement of the fraction of events with the lowest rapidity hadron detected at a rapidity greater than the target rapidity plus Δy^* for data in the shadowing region (sha, $\langle Q^2 \rangle \sim 4$, $\langle x \rangle \sim 0.01$) and the nonshadowing region (nsh, $\langle Q^2 \rangle \sim 15$, $\langle x \rangle \sim 0.05$) for xenon and deuterium. The shadowing region clearly contains more large rapidity gap events, i.e. diffractive events, than does the nonshadowing region, and more of these events occur on xenon than on deuterium. The average charge of events with no large rapidity gap is independent of x, and the x dependence of Figure 13 is due to the increasing number of diffractive events at low x, amounting to roughly 10% of the deuterium events and 20% of the xenon events for $x < 0.02$ (142).

How should these diffractive events be viewed in a parton model? Because there is no evidence of strong Q^2 dependence, they appear to be leading twist. More fundamentally, can the concept of a universal parton distribution be used to compare results of DIS with, say Drell-Yan measurements, if a large fraction of the inclusive DIS events are diffractive? Note that diffraction appears naturally in a laboratory frame description of photon-hadron interactions (196) since Fresnel diffraction occurs from any absorbing medium.

4.8 *Beyond $x = 1$*

On the proton, x cannot attain a value greater than 1.0, so nuclear structure functions at $x > 1$ must depend sensitively on the nuclear dynamics. This condition requires measurements to be performed at low energy loss—even less than the quasielastic scattering peak—and sufficiently high Q^2 in order to distinguish correlated scattering from multiple nucleons (either meson-exchange processes or effects of initial-state correlations) from partonic effects. Low Q^2 data showing features of either a nucleonic (y scaling) or a partonic mechanism (ξ scaling) at work are available from SLAC (125, 197–199). The only high Q^2 data ($Q^2 > 50$) are from the BCDMS collaboration (135) and involve carbon ($.85 < x < 1.30$). The structure functions could be fitted with an exponential [$\sim e^{-(16.5\pm0.6)x}$] form with no apparent Q^2 dependence. One must remember that as a consequence of QCD we expect substantial logarithmic slopes, $d \ln F_2 / d \ln Q^2$, as x approaches 1. Additional evidence suggests large higher-twist effects here—even on the proton.

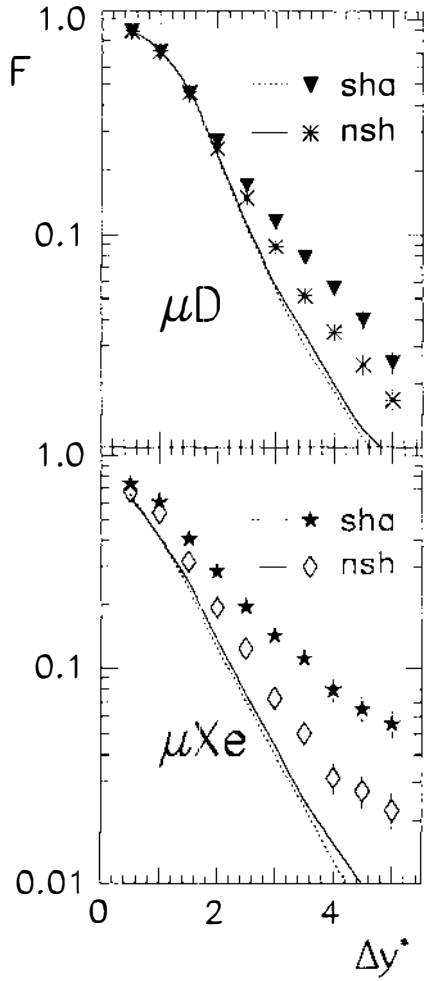

Figure 14 The fraction F of events from deep-inelastic muon scattering from xenon and deuterium targets with the slowest detected hadron at a rapidity greater than the target rapidity by Δy^* for events with $x > 0.02$ (nsh) and events with $x < 0.02$ (sha) (142). The curves are the expectations from string fragmentation models.

5. RECENT THEORETICAL DEVELOPMENTS

Here we review some recent theoretical progress in the study of the quark distributions of nuclei.

5.1 *N-N Correlations in Nuclei*

Short-range correlations (SRCs) in a nucleus create a high-momentum component in the nucleon wavefunction (200). Uchiyama & Saito (82) were probably the first to use the wavefunctions given by the Faddeev equation with a realistic N-N potential to study the EMC ratios for ^{3}He and ^{3}H. The realistic wavefunction involves all amplitudes of final excited states. Ciofi degli Atti & Liuti (201) subsequently presented calculations for a range of systems, from few-body systems to nuclear matter, using nucleon spectral functions given by realistic nuclear forces. They pointed out that SRCs play an important role in fitting the EMC ratios but that a systematic discrepancy remains between the calculations and experiments for $0.5 < x < 0.9$ (see 83 and 202). These authors also calculated that the nuclear structure functions for three-nucleon systems in the region of $x > 1$ are very sensitive to the correlation structure of the nucleon spectral function.

The fact that multiquark configurations contribute primarily to nuclear structure functions at large x (see Section 3.1) raises the question of how to distinguish this contribution from that of conventional nucleon-nucleon correlations. Many theoretical works stemmed from this question [see e.g. Frankfurt & Strikman (203), Araseki & Fujita (204), Saito & Uchiyama (69), Saito (83), Akulinichev & Shlomo (205), Anisovich et al (87), Guoju & Irvine (206), Rozynek & Birse (207), Liuti (208), Kaptari et al (209), Carlson & Lassila (210), and Atti & Simula (211)]. Although some data on the structure function of ^{12}C for $x > 1$ have been gathered by SLAC and BCDMS (see Section 4.8), they are not sufficient to provide conclusive results. Good deep-inelastic data for $x > 1$ over a wide range of Q^2 and A will be required to clarify the role of higher twist in this region.

5.2 *Beyond the Impulse Approximation*

As explained in Section 3.3, the standard approach to the calculation of the nuclear structure function based on the impulse approximation leads to a simple convolution of the structure function of the free nucleon with the light-cone momentum distribution of the bound nucleon (see Equation 49). While this attack on the problem has had some success, it is essential to go beyond the impulse approximation to test its reliability. In this regard, two interesting observations were made recently. The first is rather technical and involves the Dirac structure of the off-shell nucleon structure function. The second is very

ambitious and still in the early stages. Nevertheless, this latter development has led to an important qualitative discovery that is the focus of the next section.

5.2.1 RELATIVISTIC CORRECTIONS In order to derive the usual convolution formula for nuclear DIS, the nucleon is treated implicitly as an elementary particle. That is, in the Bjorken limit, the Dirac structure of the operator describing the structure of the nucleon, $\hat{W}^{\mu\nu}$, is assumed to be either $\hat{1}W^{\mu\nu}$ or $\not{q}W^{\mu\nu}$. This structure leads quite naturally to a convolution formula. Of course, the fact that the nucleon has a nontrivial structure function means that it is not pointlike. As a result, it does not have trivial Dirac structure either.

A recent, systematic investigation by Melnitchouk et al (212) showed that, in the Bjorken limit, the most general structure of $\hat{W}^{\mu\nu}$ was in fact

$$\hat{W}^{\mu\nu} = P_T^{\mu\nu}[\chi_0(p,q) + \not{p}\chi_1(p,q) + \not{q}\chi_2(p,q)], \qquad 72.$$

where $P_T^{\mu\nu}$ is the usual transverse projector

$$P_T^{\mu\nu} = \tilde{g}^{\mu\nu} + \frac{\tilde{p}^\mu \tilde{p}^\nu}{\tilde{p}^2} \qquad 73.$$

(cf Equation 2) and where the functions $\chi_i(p,q)$ are determined by the structure of the nucleon. Thus whereas the free structure function involves one linear combination:

$$F_2^{\text{free}} \propto m\chi_0 + m^2\chi_1 + p\cdot q\chi_2, \qquad 74.$$

which is obtained by tracing $\hat{W}^{\mu\nu}$ with $(\not{p}+m)$, in a nucleus, where the nucleon propagator is $(\not{A}+B)$, we find

$$F_2^{\text{bound}} \propto B\chi_0 + A\cdot p\chi_1 + A\cdot q\chi_2, \qquad 75.$$

which is not proportional to F_2^{free}.

The practical significance of this breakdown has been studied in detail for the deuteron. This approach requires a covariant description of the DNN vertex as well as of the off-shell nucleon structure function. For the former, we use the vertex of Reference 213. For the latter, Melnitchouk et al (212) calculated the functions $\chi_i(p,q)$ in terms of a set of covariant $N \to q$ (diquark) vertices. The diquark states were, of course, either scalar or pseudovector, and their masses were chosen, in line with the work of Close & Thomas (214), to reflect the mass splitting needed in low-energy phenomenology. Finally, the parameters of the covariant vertex functions were chosen to reproduce the free nucleon data.

The major result of this study was that, at least for the weakly bound deuteron, the difference between an optimal convolution formula and the full calculation was less than 2% for $x < 0.9$. In contrast, for $x > 1$, the off-shell corrections

start to dominate. Clearly, any precision extraction of the neutron structure function from deuterium data should take into account all nuclear effects, including this off-shell effect. For a real nucleus, the size of this effect is unknown and certainly should be a high priority for further investigation.

Other developments with respect to relativistic treatments are listed in References 213 and 215–219. Sawicki & Vary (220) studied the off-shell corrections to the parton model and discussed the violation of the Gottfried sum rule and dilepton suppression in the nuclear Drell-Yan process. Kulagin et al (221) also investigated these off-shell corrections in nuclear DIS.

5.2.2 NUCLEAR BINDING REEXAMINED The differences between the instant-form dynamics (IFD) and light-front dynamics (LFD) approaches (see Section 3.3.2) to the problem of nuclear binding may appear minor but are in fact profound. Problems of covariance are related to the nonexistence of single-particle four-momentum operators in bound systems. If one uses nonrelativistic nuclear input such as spectral functions, consistency is an important issue. In LFD, the particles are on-mass-shell, and there are no off-shell ambiguities. However, with the exception of the deuteron (222), we have little or no experience in calculating the wavefunction of a realistic nucleus in LFD. In LFD, the loss of momentum by bound nucleons can be treated only by including extra Fock components in the nuclear wavefunction so that the momentum of the whole nucleus is effectively spread over more degrees of freedom, e.g. the mesons responsible for binding (27). Conversely, in IFD we have a wealth of knowledge to draw upon in the field of nuclear dynamics. However, corrections such as the off-shell variation of the structure function described above pose more of a problem in IFD.

In addition to the issue of relativistic corrections, the validity of the impulse approximation in treating the effect of nuclear binding in IFD must also be examined. Here, one must go beyond the impulse approximation, which requires not only a method of calculating (at least the leading twist) parton distributions for a given quark model but also a realistic quark model for a nucleus. With regard to the former, formal expressions for the twist-2 parton distributions outlined in Section 2.6 have been successfully applied to the MIT bag model (24). The resulting quark/parton distributions for the free nucleon give a reasonably good description of the world data (24).

The latter requirement is somewhat more elusive, because one really needs a quark-based model that produces a reasonable fit to nuclear saturation properties. At least for infinite nuclear matter, the model developed by Guichon (223) and others is ideal. It is based on a simple model wherein quarks confined in MIT bags self-consistently exchange scalar and vector mesons. Formally, the model can be written exactly like the Walecka model (quantum hadrodynamics)

(224) but with the self-consistency condition for the mean scalar field altered by the response of the nucleon's internal structure. Remarkably, this extra degree of freedom enables the model to reproduce the observed incompressibility of nuclear matter (225, 226), a task that simple mean-field models based on nucleons alone cannot accomplish.

Because the model has thus far been restricted to nuclear matter, it has been applied only to DIS from finite nuclei using the local-density approximation (227, 228):

$$q_A^{(2)}(x) = \int d^3r \rho_A(r) q_{N/A}^{(2)}[x, k_F(r)], \qquad 76.$$

where $\rho_A(r)$ is the nuclear density distribution of the nucleus A and the distribution of valence quarks in nuclear matter is given by

$$q_{N/A}^{(2)}[x, k_F(r)] = \int_x^A dy \frac{1}{y} f_{N/A}[y, k_F(r)] q_N^{(2)}\left[\frac{x}{y}, k_F(r), \mu^2\right]. \qquad 77.$$

Here, k_F is the local Fermi momentum given by $\rho_A(r) = 2/(3\pi^2)k_F(r)^3$. Fermi motion is incorporated as a convolution of the nucleon momentum distribution in the nucleus, $f_{N/A}[y, k_F(r)]$, with the quark distribution of the bound nucleon. The latter is given in terms of the nucleon bag model with scalar and vector mean-fields. For a free nucleon, the dominant intermediate state is a two-quark bag. For nuclei, the dominant intermediate state is the two-quark bag state bound to the residual $(A - 1)$ nucleons. Within this model, the usual impulse approximation, in which nucleon binding is taken into account, the energy of interaction of the intermediate two-quark bag with the rest of the nucleus is ignored. As shown in Figure 15, the result is dramatic, with the impulse approximation overestimating the effect of binding by a factor of two or three (228).

This outcome is physically very sensible. The binding of the nucleon is the result of the attractive scalar mean field experienced by its three constituent quarks. By ignoring the binding of the pair of spectator quarks, that is, by treating the quarks as though they were free in the nucleus, one assumes that the kinematics of the hard scattering of the quark struck by the virtual photon carries the binding of all three quarks. This is clearly not the right physical picture.

While the quark model used to illustrate this point is somewhat crude and needs to be extended to finite nuclei (229), the physical insight gained is much more general. The good news is that nuclear DIS can be used to measure the energy and momentum of the quarks—not the nucleons—in nuclei. Unfortunately, in regard to performing the calculation, this is also the bad news.

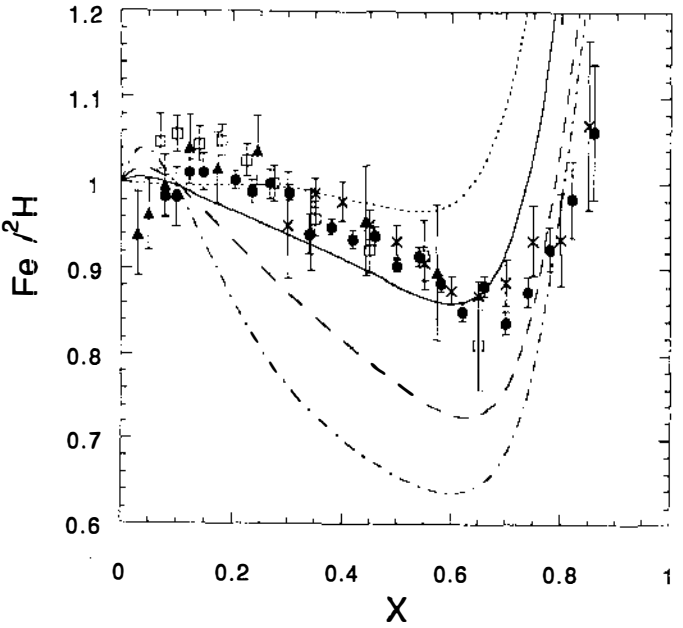

Figure 15 EMC ratio of iron to deuterium (228). The solid and dashed curves show the full calculation and that in the impulse approximation, respectively. The dotted and dot-dashed curves indicate the calculations in which the quark degrees of freedom and the center-of-mass correction to the nucleon bag are, respectively, ignored. The bag radius of the free nucleon is 0.6 fm.

5.3 *The Role of Virtual Pions*

On the one hand, in view of the role of the intermediate-range attraction in the NN force in nuclear binding and the fact that this part of the force is well understood in terms of two-pion exchange, the pion model (see Section 3.3.3) is expected to play a role in the EMC effect. On the other hand, several attempts to find an enhancement of the pion field in nuclei have been unsuccessful. In the first of these tests, the polarization transfer $(\vec{p}, \vec{n})$ reaction was used to look for an enhancement of the longitudinal isovector response of the nucleus (see Equation 57). Until recently, the findings were uniformly negative (101, 230). However, previous tests have usually relied not on the absolute value of the longitudinal response but on its ratio to the transverse response. Recent work has suggested that the problem may have caused by a larger-than-expected transverse response rather than by a suppression of the longitudinal response (231). Indeed, in this experiment, the longitudinal response was consistent (albeit with fairly large errors) with expectations based on the random-phase approximation (RPA). This topic clearly requires more experimental work.

The second approach to testing this model involves the Drell-Yan process (see Section 4.5). As we saw in Figure 9, no evidence exists for an enhancement of the antiquark distribution in heavier nuclei, as is indicated by the pion model. This important result, together with the negative results for the longitudinal response, was used to effectively rule out the pion model. However, now that the conclusion regarding the isovector longitudinal response has changed, the Drell-Yan data must be examined in more detail. In particular, we need to determine how well shadowing in the timelike region is really understood and, more generally, how the enhancement over the parton-model cross section might vary with x_1, x_2 and A.

5.4 *Nuclear Shadowing Revisited*

As described in Section 3.4, nuclear shadowing that scales was anticipated very early on (111). However, vector dominance suggests that at low Q^2, a hadronic component of the virtual photon is present whose interaction with a nucleus would be shadowed but would certainly not scale. [For a recent review of the subtlety of such arguments based on vector meson dominance (VMD), we refer the reader to O'Connell et al (114).] The experimental data, which were presented in Section 4.7, cover an enormous range of x (as low as 10^{-4}) and Q^2 (as low as 0.3 GeV^2). One of the challenges that investigators have recently begun to address is the development of a unified theoretical treatment of the shadowing region that incorporates the physics of both the partonic and hadronic regimes.

To develop a complete theory of nuclear shadowing requires an enormous range of physics, from the nature of the Pomeron and color transparency to the nonperturbative structure of hadrons. At the phenomenological level, a number of groups (192, 193, 232–234) have suggested a simple two-phase treatment, i.e. the VMD model for low Q^2 and virtual photon interactions through the Pomeron for high Q^2. The total shadowing value is then provided by the combination of the two effects. They showed that this model can give a quantitative description of the observed shadowing for various nuclei, including the deuteron.

According to this physical picture, the virtual photon interacts with the nuclear target via its fluctuations into $q\bar{q}$ pairs. If the virtuality for the photon is large, then the fluctuation is spatially small and a parton description is relevant. Conversely, if the virtuality is small, a VMD-based description is appropriate. [This approach is similar to the model adopted by Kwiecinski & Badelek (232); see also Reference 235.]

The empirical basis of the VMD model is the observation that photon-hadron processes are remarkably similar to pure hadronic reactions. A virtual hadronic (vector meson, v) component in the photon contributes to nuclear structure

functions for small x at low Q^2. The correction to the nuclear structure function (per nucleon) may be given as (see also References 236 and 239):

$$\delta^{\mathrm{V}} F_2^{\mathrm{A}}(x, Q^2) = \frac{Q^2}{\pi \mathrm{A}} \sum_{v=\rho^0,\omega,\phi} \frac{m_v^4 \delta\sigma_{v\mathrm{A}}}{f_v^2 \left(Q^2 + m_v^2\right)^2}, \qquad 78.$$

dequation where m_v is the vector meson mass, f_v is the coupling strength between the meson and the photon, and $\delta\sigma_{v\mathrm{A}}$ is the shadowing correction to the vA cross section, which may be given by the eikonal approximation. For light nuclei, the double scattering of vector mesons from two nucleons is dominant. Multiple rescattering may become more important as A increases. As Equation 78 shows, this contribution to shadowing does not scale. In the pure hadronic VMD picture, scaling can be recovered only from off-diagonal interference between vector meson states.

For high Q^2, a partonic description may be efficient. In the Regge region ($Q^2/x \gg Q^2$), the structure function may be described in terms of the interaction of the virtual photon with the Pomeron ($\mathcal{P}$) through its structure function $F_2^{\mathcal{P}}(x_{\mathcal{P}}, Q^2)$, where $x_{\mathcal{P}}$ is the fraction of the Pomeron's momentum carried by the struck quark (193, 232, 237, 240–242). In diffractive DIS from nuclei, the shadowing correction to F_2^{A} from Pomeron exchange may be written using a convolution form:

$$\delta^{\mathcal{P}} F_2^{A}(x, Q^2) = \frac{1}{A} \int_{y_{\min}}^{A} dy f_{\mathcal{P}/\mathrm{A}}(y) F_2^{\mathcal{P}}\left(x_{\mathcal{P}}, Q^2\right). \qquad 79.$$

Here, $y_{\min} = x(1 + M_{X_0}^2/Q^2)$, where $M_{X_0}^2 \simeq 1.5\ \mathrm{GeV}^2$ and where $f_{\mathcal{P}/\mathrm{A}}(y)$ describes the y distribution of the exchanged $\mathcal{P}$ given by the eikonal approximation. The total shadowing correction is thus given by Equations 78 and 79. In this model, the apparent saturation of shadowing at $x \lesssim 10^{-3}$ in the ratio of xenon to deuterium (see Figure 4 and Section 4.7) is naturally explained.

A much more ambitious approach is to allow the virtual photon to dissociate into a $q\bar{q}$ pair and then to model the interaction of that pair with the nucleus. Whether the pair interacts strongly or not is governed by its transverse separation. The limit of small transverse separation corresponds to color transparency, i.e. to a vanishing cross section for the interaction of the pair with the nucleus. On the other hand, for a transverse separation greater than or equal to a typical hadron size (~ 1 fm), the cross section saturates at a typical hadronic cross section. The advantage of this approach is that the frozen approximation is valid and the cross section is diagonal in the transverse separation. In applying these ideas, Frankfurt & Strikman (237), Nikolaev & Zakharov (241), and Piller et al (233) all noticed an important subtlety, namely that the transverse size depends on both the invariant mass of the quark pair and the sharing of their longitudinal

momentum fraction. This observation has important consequences for the Q^2 dependence of the results. No doubt this problem will be an area of intense study over the next few years as both the data and the theoretical understanding improve.

6. OUTLOOK

The decade since the discovery of the EMC effect has seen many important experimental and theoretical developments. Dramatic new features of nuclear structure, such as quark percolation or partial deconfinement, unfortunately remain highly speculative. Nevertheless, we largely know which issues must be addressed before we can test such ideas, and powerful techniques have been developed to resolve them.

We now understand that nuclear DIS probes the energy and momentum distribution of quarks in the nucleus. The treatment of binding and Fermi motion within IFD has become very sophisticated. For example, nucleon-nucleon correlations, off-shell effects, and corrections to the impulse approximation have all received serious attention. However, the explicit quark models of nuclear structure must be extended to finite nuclei and used to calculate nuclear structure functions. The alternative approach of LFD has the distinct advantage of finessing off-mass-shell effects and needs to be developed further. Consistent, realistic light-front wavefunctions (including several Fock components and fitting low energy observables) on nuclei are urgently needed.

As we have demonstrated in this review, a considerable body of data has been accumulated on nuclear parton distributions. Increasingly, the experimental outlook will involve alternative, hard probes with specific sensitivities to the quark-flavor distributions and the glue. Most importantly, convincing studies of the nuclear gluon distributions at all x ranges are needed. The probes of choice seem to be: (*a*) direct photon production in pA collisions; (*b*) higher-statistics studies of heavy-quark production in DIS and in pA collisions; (*c*) high-statistics, two forward–jet production in DIS and in pA collisions; and (*d*) more precise measurements of σ_L/σ_T.

Possibilities for the first three will be enhanced when high-energy proton-nucleus collisions can be studied at the Relativistic Heavy-Ion Collider, RHIC. All three require systematic study, as substantive questions about the reaction mechanism must be addressed before model-independent sensitivity to the gluon distribution can be demonstrated. Unfortunately, no program is in place to extend the measurements of σ_L, which are admittedly very difficult to perform, to the low x region.

The emphasis in quark distributions will be on flavor distributions and on the extension to higher x:

- The measurements of antiquark distributions must be extended to lower and higher x with Drell-Yan measurements. At present, these measurements can be performed at FNAL and CERN. With the new FNAL Main Injector, higher x values should also be possible. RHIC can also make important contributions in this area, primarily through the larger $|Q^2|$ at the same x as currently measured in DIS.

- The nature of the small bump in the region of x around 0.1–0.2 must be clarified, and the low-energy experiments, such as polarization transfer $(\vec{p}, \vec{n})$ reactions, must be extended in order to pin down the nuclear isovector, longitudinal response.

- With Drell-Yan measurements, one can focus on the differences $\bar{d}_p - \bar{u}_p$ that have been observed and use $\bar{u}_p - \bar{d}_n$ and $d_p - u_n$ to test charge symmetry.

- High Q^2 data at high x should be a top priority. Here, systematics may be very important for examining the higher-twist contributions. On the theoretical side, more work is needed on the off-shell corrections, which tend to dominate at large x.

- The neutrino (CCFR) and muon (NMC) data significantly disagree at low x ($\sim$20% at $x < 0.08$). Attributing this difference to the strange quark contribution is not consistent with the CCFR multimuon measurement of the strange quark distributions. It would be very interesting to be able to extract the A-dependence of the strange quark distribution. In this regard, new, high-statistics neutrino measurements are under way at FNAL.

The importance of diffractive events in the shadowing region points to the power of large-acceptance hadron detection in DIS. More data are needed on the role of diffraction in other hard processes, particularly in Drell-Yan reactions and neutrino scattering, and more precise experimental tests of factorization and the universality of parton distributions should be performed as well. The deep-inelastic studies would be significantly more powerful if heavy ions could be accelerated with sufficient intensity in HERA. From a theoretical point of view, more work is needed on the connection between explicit quark models, based on quark rescattering, and the more phenomenological approaches involving VMD, double- and triple-Pomeron exchange, and meson-exchange corrections.

Measurements of the hadronic final states may also allow other nuclear effects to be separated. A few important examples are:

- Studies of the A-dependence of the transverse momentum $\mathbf{k}_T$ from azimuthal asymmetry studies of L-T interference.

- At high x, identification of reactions occuring on loosely bound nucleons compared with those on deeply bound nucleons.
- Observation of the participation of a correlated pair of nucleons by direct detection of the high-momentum partner in the backward hemisphere.

The future availability of high-energy ($\geq$ 20 GeV) high duty factor electron facilities such as the Electron Laboratory for Europe or of an upgraded CEBAF will likely be necessary in order to capitalize on these opportunities.

ACKNOWLEDGMENTS

It is a pleasure to thank the many colleagues who have contributed to our understanding of the issues presented here. We would like to thank particularly SD Bass, F Coester, S Daté, JT Londergan, H Melanson, W Melnitchouk, G Piller, J Qiu, H Schellman, AW Schreiber, AI Signal, M Strikman, H Sumiyoshi, T Suzuki, and T Uchiyama. This work was supported in part by the Australian Research Council and the US Department of Energy, Nuclear Science Division, under contract W-31-109-ENG-38.

Literature Cited

1. AubertJJ, etal. EMCCollaboration. *Phys. Lett. B* 123:275 (1983)
2. Gomez J, et al. *Phys. Rev. D* 49:4348 (1994)
3. Dasu S, etal. *Phys. Rev. D* 49:5641 (1994)
4. Benvenuti AC, et al. BCDMS Collaboration. *Phys. Lett. B* 189:483 (1987)
5. Ashman J, et al. EMC Collaboration. Z. *Phys. C* 57:211 (1993)
6. Ashman J, et al. EMC Collaboration. *Phys. Lett. B* 202:603 (1988)
7. Sather E. *Phys. Lett. B* 274:433 (1992)
8. Rodionov EN, Thomas AW, Londergan JT. *Mod. Phys. Lett. A* 9:1799 (1994)
9. Dasu S, et al. *Phys. Rev. Lett.* 60:2591 (1988)
10. Morfin JG. *New Directions in Fermilab Neutrino Physics*, ed. R Bernstein, et al, p. 13. Batavia: Fermilab (1988)
11. Close FE. *An Introduction to Quarks and Partons.* New York: Academic (1979)
12. Leader L, Predazzi E. *An Introduction to Gauge Theories and the New Physics.* Cambridge: Cambridge Univ. Press (1982)
13. Muta T. *Foundations of Quantum Chromodynamics,* World Scientific Lecture Notes in Physics, Vol. 5. Singapore: World Scientific (1987)
14. Sachrajda CT. *Gauge Theories in High Energy Physics,* ed. MK Gaillard, R. Stora. Amsterdam: North Holland (1983)
15. Yndurain F. *Quantum Chromodynamics.* Berlin: Springer (1983)
16. Alonso JL, Tarrach R, eds. *Quantum Chromodynamics.* Berlin: Springer (1980)
17. Altarelli G. *Phys. Rep.* 81:1 (1982)
18. Craigie NS, et al. *Phys. Rep.* 99:69 (1983)
19. Lissia M. *Nucl. Phys. A* 555:272 (1993)
20. Martinelli G, Sachrajda CT. *Phys. Lett.* B217:319 (1988)
21. Jaffe RL. *Nucl. Phys. B* 229:205 (1983)
22. Thomas AW. *Prog. Nucl. Part. Phys.* 11:325 (1984)
23. Thomas AW. *Prog. Part. Nucl. Phys.* 20:21 (1988)
24. Signal AI, Thomas AW. *Phys. Rev D*

40:2832 (1989); Schreiber AW, Signal AI, Thomas AW. *Phys. Rev. D* 44:2653 (1991)
25. Pirner HJ. *Prog. Nucl. Part. Phys.* 13:361 (1984)
26. Barone C, Predazzi E. *Ann. Phys. Fr.* 12:525 (1987)
27. Berger EL, Coester F. *Annu. Rev. Nucl. Part. Sci.* 37:463 (1987)
28. Frankfurt LL, Strikman MI. *Phys. Rep.* 160:235 (1988); *Modern Topics in Electron Scattering*, ed. B Frois, I Sick, p. 762. Singapore: World Scientific (1991)
29. Rith K. Z. *Phys. C* 38:317 (1988)
30. Bickerstaff RP, Thomas AW. *J. Phys. G* 15:1523 (1989)
31. Roberts RG. *The Structure of the Proton*. Cambridge: Cambridge Univ. Press (1990)
32. Barone V, et al. *Z. Phys. C* 58:541 (1993)
33. Arneodo M. *Phys. Rep.* 240:301 (1994)
34. Krzywicki A. *Phys. Rev. D* 14:152 (1976)
35. Sivers D. *Annu. Rev. Nucl. Part. Sci.* 32:149 (1982)
36. Pirner HJ, Vary JP. *Phys. Rev. Lett.* 46:1376 (1981)
37. Carlson CE, Havens TJ. *Phys. Rev. Lett.* 51:261 (1983)
38. Daté S, Nakamura A. *Prog. Theor. Phys.* 69:565 (1983)
39. Daté S. *Prog. Theor. Phys. Lett.* 70:1682 (1983)
40. Faissner H, Kim BR. *Phys. Lett. B* 130:321 (1983)
41. Daté S, et al. *Phys. Rev. Lett.* 52:2344 (1984)
42. Vary JP. *Nucl. Phys. A* 418:195c (1984)
43. Faissner H, Kim BR, Reithler H. *Phys. Rev. D* 30:900 (1984)
44. Chemtob M, Peschanski R. *J. Phys. G* 10:599 (1984)
45. Diasde Deus J, Pimenta M, Varela J. *Phys. Rev. D* 30:697 (1984)
46. Clark BC, et al. *Phys. Rev. D* 31:617 (1985)
47. Kondratyuk LA, Shmatikov MZh. *Z. Phys. A* 321:301 (1985)
48. Vary JP, Harindranath A. *Lecture Notes in Physics*, ed. BL Berman, B Gibson, 260:422. Berlin: Springer-Verlag (1986)
49. Kisslinger LS, Johnson MB. *Phys. Rev. C* 36:1081 (1987)
50. Lassila KE, Sukhatme UP. *Phys. Lett. B* 209:343 (1988)
51. Barshay S, Rein D. *Z. Phys. C* 46:215, 696 (erratum) (1990)
52. Miller GA. *Quarks and Nuclei*, ed. W Weise, Vol. 1. Singapore: World Scientific (1984)
53. Nachtmann O, Pirner HJ. *Z. Phys. C* 21:277 (1984)
54. Close FE, Roberts RG, Ross GG. *Phys. Lett. B* 129:346 (1983)
55. Jaffe RL, et al. *Phys. Lett. B* 134:449 (1984); Close FE, Roberts RG, Ross GG. *Phys. Lett. B* 142:202 (1984); Close FE, et al. *Phys. Rev. D* 31:1004 (1985); Close FE, Roberts RG, Ross GG. *Phys. Lett. B* 168:400 (1986), *Nucl. Phys. B* 296:582 (1988); Close FE, Roberts RG. *Phys. Lett. B* 213:91 (1988)
56. Gupta S, Banerjee B, Godbole RM. *Z. Phys. C* 28:483 (1985)
57. Bickerstaff RP, Miller GA. *Phys. Lett. B* 168:409 (1986)
58. Bickerstaff RP, Thomas AW. *Phys. Rev. D* 35:108 (1987)
59. Kumano S. *Phys. Rev. C* 48:2016 (1993), *Phys. Lett. B* 298:171 (1993), *Phys. Rev. C* 50:1247 (1994)
60. Chanfray G, Nachtmann O, Pirner HJ. *Phys. Lett. B* 147:249 (1984)
61. Williams AG, Thomas AW. *Phys. Lett. B* 154:320 (1985); Chanfray G, Pirner HJ. *Phys. Rev. C* 35:760 (1987)
62. Close FE, Roberts RG, Ross GG. *Nucl. Phys. B* 296:582 (1988)
63. Cleymans J, Thews RL. *Phys. Rev. D* 31:1014 (1985)
64. Sick I. *Nucl. Phys. A* 434:677c (1985), *Phys. Lett. B* 157:13 (1985)
65. Mulders PJ. *Phys. Rev. Lett.* 54:2560 (1985)
66. West GB. *Phys. Lett. B* 37:509 (1971), *Ann. Phys.* 74:464 (1972)
67. Atwood WB, West GB. *Phys. Rev. D* 7:773 (1973)
68. Bodek A, Ritchie JL. *Phys. Rev. D* 23:1070 (1981)
69. Saito K, Uchiyama T. *Z. Phys. A* 322:299 (1985)
70. Frankfurt LL, Strikman MI. *Phys. Lett. B* 64:433 (1976), *Phys. Lett. B* 65:51 (1976), *Phys. Lett. B* 76:333 (1978), *Nucl. Phys. B* 148:107 (1979), *Phys. Rep.* 76:215 (1981)
71. Landshoff PV, Pilkinghorne JC. *Phys. Rev. D* 18:153 (1978)
72. Kusno D, Moravcsik MJ. *Phys. Rev. D* 20:2734 (1979)
73. Morley PD, Schmidt IA. *Phys. Rev. D* 34:1305 (1986); *Phys. Rev. C* 38:1356 (1988)
74. Jaffe RL. *Relativistic Dynamics and Quark-Nuclear Physics*, ed. MB Johnson, A Pickleseimer, p. 537. New York: Wiley (1985)
75. Jung H-M, Miller GA. *Phys. Lett. B* 200:351 (1988)
76. Akulinichev SV, Kulagin SA, Vagradov GM. *Pi'sma Zh. Eksp. Theor. Fiz.* 42:105 (1985), Trans. in *JETP Lett.* 42:127;

Phys. Lett. B 158:485 (1985); *J. Phys. G* 11:L245 (1985); Akulinichev SV, et al. *Phys. Rev. Lett.* 55:2239 (1985)
77. Dunne GV, Thomas AW. *Nucl. Phys. A* 446:437c (1985); *Phys. Rev. D* 33:2061 (1986); *Nucl. Phys. A* 455:701 (1986)
78. Jaffe RL. *Phys. Rev. Lett.* 50:228 (1983)
79. Llewellyn Smith CH. *Phys. Lett. B* 128:107 (1983)
80. Garcia-Canal CA, Santangelo EM, Vucetich H. *Phys. Rev. Lett.* 53:1430 (1984)
81. Birbrair BL, et al. *Phys. Lett. B* 166:119 (1986)
82. Uchiyama T, Saito K. *Phys. Rev. C* 38:2245 (1988)
83. Saito K. *Prog. Theor. Phys.* 82:18 (1989); Fukunaga A, Saito K. *Z. Phys. A* 334:473 (1989)
84. Berger EL, Coester F, Wiringa RB. *Phys. Rev. D* 29:398 (1984)
85. Berger EL, Coester F. *Phys. Rev. D* 32:1071 (1985); *Annu. Rev. Nucl. Part. Sci.* 37:463 (1987)
86. Bickerstaff RP. *Proc. Int. Conf., Taipei, Taiwan, 1988,* ed. W-YP Hwang, K-FLiu, Y Tzeng, p. 99. Singapore: World Scientific (1988)
87. Anisovic VV, Sarantsev AV, Starodubsky VE. *Nucl. Phys. A* 468:429 (1987)
88. Koltun DS. *Phys. Rev. Lett.* 28:182 (1972)
89. Frullani S, Mougey J. *Adv. Nucl. Phys.* 14:1 (1984)
90. Li GL, Liu KF, Brown GE. *Phys. Lett. B* 213:531 (1988)
91. Oelfke U, Sauer PU, Coester F. *Nucl. Phys. A* 518:593 (1990)
92. Jaffe RL. *Comments Nucl. Part. Phys.* 13:39 (1984)
93. Hoodbhoy P, Jaffe RL. *Phys. Rev. D* 35:113 (1987)
94. Spit WFM, et al. *Nucl. Phys. A* 570:472 (1994)
95. Meyer H, Mulders PJ, Spit WFM. *Nucl. Phys. A* 570:497 (1994)
96. Gurvitz SA, Rinat AS. *Weizmann Preprint WIS-94-48-PH* (1994)
97. Ericson M, Thomas AW. *Phys. Lett. B* 128:112 (1983)
98. Sullivan JD. *Phys. Rev. D* 5:1732 (1972)
99. Oset E, Toki H, Weise W. *Phys. Rep.* 83:281 (1982)
100. Abramowicz H, et al. *Z. Phys. C* 25:29 (1984)
101. Carey TA, et al. *Phys. Rev. Lett.* 53:144 (1984)
102. Cooper AM, et al. *Phys. Lett. B* 141:133 (1984)
103. Parker MA, et al. *Nucl. Phys. B* 232:1 (1984)
104. Ericson M, Thomas AW. *Phys. Lett. B* 148:191 (1984)
105. Esbensen H, Toki H, Bertsch GF. *Phys. Rev. C* 31:1816 (1985)
106. Bickerstaff RP, Birse MC, Miller GA. *Phys. Rev. D* 33:3228 (1986)
107. Chanfray G. *Proc. Int. Symp. on Weak and Electromagnetic Interactions in Nuclei,* ed. HV Klapdor, p. 431. Heidelberg: Springer-Verlag (1986)
108. Birbair BL, Levin EM, Shuvaev AG. *Nucl. Phys. A* 491:618 (1989)
109. Epele LN, et al. *Z. Phys. C* 64:285 (1994)
110. Umnikov AYu, Khanna FC, Kaptari LP. *Univ. Alberta Preprint Alberta-Thy-38-94* (1994)
111. Nikolaev NN, Zakharov VI. *Phys. Lett. B* 55:397 (1975)
112. Gribov VN. *Zh. Eksp. Thor. Fiz.* 57:1306 (1969)
113. Bauer TH, et al. *Rev. Mod. Phys.* 50:261 (1978)
114. O'Connell HB, et al. *Univ. Adelaide Preprint ADP-95-1/T168* (hep-ph/9501251)
115. Gribov LV, Levin EM, Ryskin MG. *Nucl. Phys. B* 188:555 (1981), *Phys. Rep.* 100:1 (1983)
116. Levin EM, Ryskin MG. *Yad. Fiz.* 41:472 (1985), *Sov. J. Nucl. Phys.* 41:300 (1985), *Yad. Fiz.* 41:1622 (1985), *Sov. J. Nucl. Phys.* 41:1027 (1985), and *Phys. Rep.* 189:269 (1990)
117. Brodsky SJ, Close FE, Gunion JF. *Phys. Rev. D* 6:177 (1972)
118. Mueller AH, Qiu J. *Nucl. Phys. B* 268:427 (1986)
119. Qiu J. *Nucl. Phys. B* 291:746 (1987)
120. Berger EL, Qiu J. *Phys. Lett. B* 206:141 (1988)
121. Close FE, Roberts RG. *Phys. Lett. B* 213:91 (1988)
122. Close FE, Qiu J, Roberts RG. *Phys. Rev. D* 40:2820 (1989)
123. Zhu W, Shen JG. *Phys. Lett. B* 235:170 (1990)
124. Arnold RG, et al. *Phys. Rev. Lett.* 52:727 (1984)
125. Bosted P, et al. *Phys. Rev. C* 46:2505 (1992)
126. Whitlow LW, et al. *Phys. Lett. B* 282:475 (1992)
127. Whitlow LW, et al. *Phys. Lett. B* 250:193 (1990)
128. Amaudruz P, et al. NMC Collaboration. *Phys. Lett. B* 295:159 (1992)
129. Amaudruz P, et al. NMC Collaboration. *Phys. Lett. B* 294:120 (1992)
130. Amaudruz P, et al. NMC Collaboration. *Z. Phys. C* 53:73 (1992)

131. Amaudruz P, et al. NMC Collaboration. *Nucl. Phys. B* 371:553 (1992)
132. Amaudruz P, et al. NMC Collaboration. *Z. Phys. C* 51:387 (1991)
133. Amaudruz P, et al. NMC Collaboration. *Nucl. Phys. B* 371:3 (1992)
134. Arneodo M, et al. NMC Collaboration. *Phys. Rev. D* 50:R1 (1994)
135. Benvenuti AC, et al. BCDMS Collaboration. *Z. Phys. C* 63:29 (1994)
136. Benvenuti AC, et al. BCDMS Collaboration. *Phys. Lett. B* 237:599 (1990)
137. Benvenuti AC, et al. BCDMS Collaboration. *Phys. Lett. B* 195:91 (1987)
138. Benvenuti AC, et al. BCDMS Collaboration. *Phys. Lett. B* 163:282 (1985)
139. Arneodo M, et al. EMC Collaboration. *Phys. Lett. B* 211:493 (1988)
140. Aubert JJ, et al. EMC Collaboration. *Nucl. Phys. B* 293:740 (1987)
141. Aubert JJ, et al. EMC Collaboration. *Nucl. Phys. B* 272:158 (1986)
142. Adams MR, et al. E665 Collaboration. *Z. Phys. C* 65:225 (1995)
143. Adams MR, et al. E665 Collaboration. *Z. Phys. C* 61:179 (1994)
144. Adams MR, et al. E665 Collaboration. *Fermilab Pub-95017-E.* Submitted to *Phys. Rev. Lett.* (1995)
145. Adams MR, et al. E665 Collaboration. *Phys. Rev. Lett.* 68:3266 (1992)
146. Adams MR, et al. E665 Collaboration. *Phys. Lett. B* 287:375 (1992)
147. Roberts RG, Whalley MR. *J. Phys. G* 17:D1 (1991)
148. Mo LW, Tsai YS. *Rev. Mod. Phys.* 41:205 (1969)
149. Tsai YS. *SLAC-PUB-848* (1976)
150. Akhundov AA, et al. *Sov. J. Nucl. Phys.* 26:660 (1977)
151. Bardin D, Shumeiko N. *Sov. J. Nucl. Phys.* 29:499 (1979)
152. Akhundov AA, et al. *Sov. J. Nucl. Phys.* 44:988 (1986)
153. Badelek B, et al. *Uppsala University Report No. TSL/ISV-94-0092.* Unpublished data
154. Ditzler WR, et al. *Phys. Lett. B* 57:201 (1975)
155. Stein S, et al. *Phys. Rev. D* 12:1884 (1975)
156. Bodek A, et al. *Phys. Rev. Lett.* 50:1431 (1983)
157. Bodek A, et al. *Phys. Rev. Lett.* 51:534 (1983)
158. Arneodo M, et al. EMC Collaboration. *Nucl. Phys. B* 258:249 (1985)
159. Aubert JJ, et al. EMC Collaboration. *Phys. Lett. B* 152:433 (1985)
160. Arvidson A, et al. EMC Collaboration. *Nucl. Phys. B* 246:381 (1984)
161. Adams MR, et al. E665 Collaboration. *Phys. Rev. Lett.* 69:1026 (1992)
162. Berge P, et al. Cern-Dortmund-Heidelberg-Saclay-Warsaw Collaboration. *Z. Phys. C* 49:187 (1990)
163. Allasia D, et al. Big European Bubble Chamber Collaboration. *Z. Phys. C* 28:321 (1985)
164. Jones GT, et al. BEBC Collaboration. *Z. Phys. C* 62:575 (1994)
165. Jones GT, et al. BEBC Collaboration. *Z. Phys. C* 62:601 (1994)
166. Varvell K, et al. BEBC Collaboration. *Z. Phys. C* 36:1 (1987)
167. Quintas PZ, et al. Chicago-Columbia-Fermilab-Rochester Collaboration. *Phys. Rev. Lett.* 71:1307 (1993)
168. Rabinowitz SA, et al. CCFR Collaboration. *Phys. Rev. Lett.* 70:134 (1993)
169. Kitagaki T, et al. *Phys. Lett. B* 214:281 (1988)
170. Ishii C, Saito K, Takagi F. *Phys. Lett. B* 216:409 (1989)
171. Melnitchouk W, Thomas AW, Nikolaev NN. *Z. Phys. A* 342:215 (1992)
172. Bosveld GD, Dieperink AEL, Tenner AG. *Phys. Rev. C* 45:2616 (1992)
173. Allport PP, et al. *Phys. Lett. B* 232:417 (1989)
174. Sick I, Day D. *Phys. Lett. B* 274:16 (1992)
175. Dasu S, et al. *Phys. Rev. Lett.* 61:1061 (1988)
176. Carroll T. *Observation of Nuclear Shadowing at Low X_{Bj} in Carbon, Calcium, and Lead.* Ph.D Thesis, Univ. Illinois, Chicago (1994)
177. Benvenuti AC, et al. BCDMS Collaboration. *Phys. Lett. B* 223:490 (1989)
178. Arneodo M, et al. NMC Collaboration. *Phys. Lett. B* 309:222 (1993)
179. Benvenuti AC, et al. BCDMS Collaboration. *Phys. Lett. B* 237:592 (1990)
180. Benvenuti AC, et al. BCDMS Collaboration. *Phys. Lett. B* 195:97 (1987)
181. Milsztajn A. *Proc. Workshop on Hadron Structure Functions and Parton Distributions, FNAL, 1990,* ed. DF Geesaman, et al. Singapore: World Scientific (1990)
182. Milsztajn A, et al. *Z. Phys. C* 49:527 (1991)
183. Virchaux M, Milsztajn A, *Phys. Lett. B* 274:221 (1992)
184. Matsuura T, van der Marck SC, van Neerven WL. *Nucl. Phys. B* 319:570 (1989)
185. Alde DA, et al. E772 Collaboration. *Phys. Rev. Lett.* 64:2479 (1990)
186. Nachtmann O. *Nucl. Phys. B* 78:455 (1974)
187. Georgi H, Politzer HD. *Phys. Rev. D* 14:1829 (1976)

188. Nikolaev NN, Zakharov BG. *Phys. Lett. B* 332:184 (1994)
189. Berger EL, Jones D. *Phys. Rev. D* 23:1521 (1981)
190. Baller B. *Proc. Workshop on Jet Production in Deep Inelastic Scattering on Nucleons and Nuclei, FNAL* (1993)
191. Caldwell DG, et al. *Phys. Rev. Lett.* 42:553 (1979)
192. Badelek B, Kwiecinski J. *Phys. Rev. D* 50:R4 (1994)
193. Melnitchouk W, Thomas AW. *Phys. Rev. D* 47:3783 (1993), *Phys. Lett. B* 317:437 (1993)
194. Adams MR, et al. E665 Collaboration. *Phys. Rev. Lett.* In press (1995)
195. Derrick M, et al. *Phys. Lett. B* 332:228 (1994)
196. Nikolaev NN, Zakharov BG, Zoller VR. *KFA-IKP(TH)-1994-13.* Unpublished
197. Filippone BW, et al. *Phys. Rev. C* 45:1582 (1992)
198. Rock S, et al. *Phys. Rev. D* 46:24 (1992)
199. Day D. *Nucl. Phys. A* 478:397c (1988)
200. Mahaux C, Sartor R. *Adv. Nucl. Phys.* 20:1 (1991)
201. Ciofi degli Atti C, Liuti S. *Phys. Lett. B* 225:215 (1989), *Phys. Rev. C* 41:1100 (1990), *Phys. Rev. C* 44:R1269 (1991)
202. Dieperink AEL, Miller GA. *Phys. Rev. C* 44:866 (1991)
203. Frankfurt LL, Strikman MI. *Phys. Lett. B* 69:93 (1977), *Nucl. Phys. B* 181:22 (1981), *Phys. Lett. B* 114:345 (1982)
204. Araseki H, Fujita T. *Nucl. Phys. A* 439:681 (1985)
205. Akulinichev SV, Shlomo S. *Phys. Rev. C* 33:1551 (1986)
206. Guoju H, Irvine JM. *J. Phys. G* 15:147 (1989)
207. Rozynek J, Birse MC. *Phys. Rev. C* 38:2201 (1988)
208. Liuti S. *Phys. Rev. C* 47:R1854 (1993)
209. Kaptari LP, Umnikov AYu, Kämpfer B. *Phys. Rev. D* 47:3804 (1993)
210. Carlson CE, Lassila KE. *Phys. Lett. B* 317:205 (1993)
211. Ciofi degli Atti C, Simula S. *Phys. Lett. B* 325:276 (1994)
212. Melnitchouk W, Schreiber AW, Thomas AW. *Phys. Rev. D* 49:1183 (1994), *Phys. Lett. B* 335:11 (1994)
213. Gross F, Liuti S. *Phys. Rev. C* 45:1374 (1992)
214. Close FE, Thomas AW. *Phys. Lett. B* 212:227 (1988)
215. Nakano K. *Nucl. Phys. A* 511:664 (1990)
216. Mulders PJ, Schreiber AW, Meyer H. *Nucl. Phys. A* 549:498 (1992)
217. Kaptari LP, Kazakov KYu, Umnikov AYu. *Phys. Lett. B* 293:219 (1992)
218. Birse MC. *Phys. Lett. B* 299:186 (1993)
219. Umnikov AYu, Khanna FC. *Phys. Rev. C* 49:2311 (1994)
220. Sawicki M, Vary JP. *Phys. Rev. Lett.* 71:1320 (1993)
221. Kulagin SA, Piller G, Weise W. *Phys. Rev. C* 50:1154 (1994)
222. Chung PL, et al. *Phys. Rev. C* 37:2000 (1988)
223. Guichon PAM. *Phys. Lett. B* 200:235 (1988)
224. Saito K, Thomas AW. *Phys. Lett. B* 327:9 (1994)
225. Saito K, Thomas AW. *Phys. Lett. B* 335:17 (1994), *Phys. Rev. C.* 51:2757 (1995)
226. Thomas AW, Saito K. *Proc. Int. Conf. on Physics with GeV-Particle Beams, Jülich, August 1994* (1994)
227. Saito K, Michels A, Thomas AW. *Phys. Rev. C* 46:R2149 (1992); Thomas AW, Saito K, Michels A. *Aust. J. Phys.* 46:3 (1993)
228. Saito K, Thomas AW. *Nucl. Phys. A* 574:659 (1994)
229. Guichon PAM, Saito K, Thomas AW. In preparation (1995)
230. Chen XY, et al. *Phys. Rev. C* 47:2159 (1993)
231. Taddeucci TN, et al. *Phys. Rev. Lett.* 73:3516 (1994)
232. Kwiecinski J, Badelek B. *Phys. Lett. B* 208:508 (1988)
233. Piller G, Weise W. *Nucl. Phys. A* 532:271c (1991), *Phys. Rev. C* 42:R1834 (1990)
234. Barone V, et al. *Phys. Lett. B* 321:137 (1994)
235. Bartels J, Ryskin MG. *Z. Phys. C* 60:751 (1993)
236. Shaw G. *Phys. Lett. B* 228:125 (1989)
237. Frankfurt LL, Strikman MI. *Nucl. Phys. B* 316:340 (1989); Frankfurt LL, Strikman MI, Liuti S. *Phys. Rev. Lett.* 65:1725 (1990)
238. Zhu W, et al. *Phys. Lett. B* 317:200 (1993)
239. Donnachie A, Landshoff PV. *Phys. Lett. B* 191:309 (1987)
240. Brodsky SJ, Lu HJ. *Phys. Rev. Lett.* 64:1342 (1990)
241. Nikolaev NN, Zakharov BZ. *Phys. Lett. B* 260:414 (1991), *Z. Phys. C* 49:607 (1991), 53:331 (1992)
242. Levin E, Müsthoff M. *Phys. Rev. D* 50:4306 (1994)